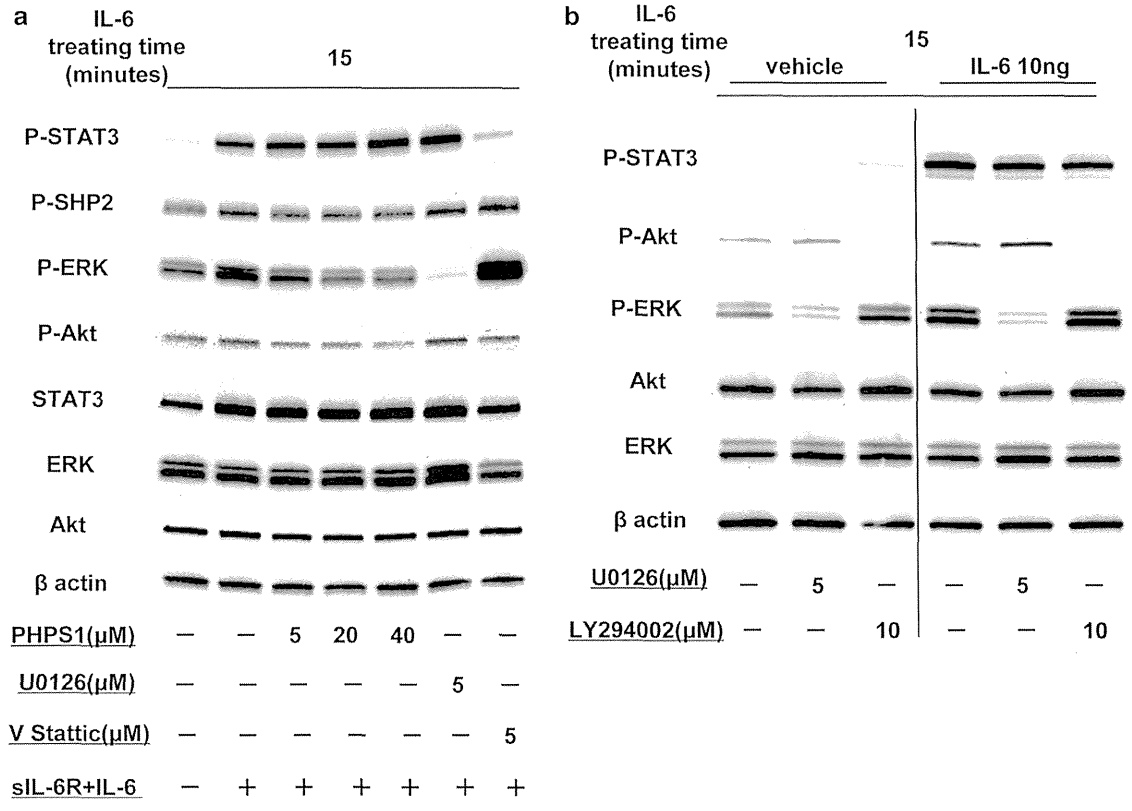

Fig. 4 IL-6-induced activation of ERK was enhanced by blocking the STAT3 signaling pathway, and IL-6-induced ERK and Akt signaling pathways negatively regulated each other reciprocally. **a** MC3T3-E1 cells were stimulated with 10 ng/ml IL-6 and 100 ng/ml sIL-6R (15 min) after pretreatment either with PHPS1 (5, 20, 40 μM; 1 h), with U0126 (5 μM; 1 h), or with V Stattic (5 μM; 1 h), and the cell lysates were subjected to Western blotting. PHPS1 inhibited IL-6-induced phosphorylation of ERK and Akt to the constitutive level, but not of STAT3. IL-6-induced activation of ERK was enhanced by V Stattic. **b** MC3T3-E1 cells were treated with vehicle or with 10 ng/ml IL-6 and 100 ng/ml sIL-6R (15 min) after pretreatment either with U0126 (5 μM; 1 h) or with LY294002 (10 μM; 1 h), and the cell lysates were subjected to Western blotting. Both constitutive and IL-6-induced phosphorylation of Akt and ERK were enhanced by treatment with U0126 and LY294002, respectively. Representative data from at least three independent experiments are shown

The negative effect of IL-6/sIL-6R on the expression of osteoblastic genes (Runx2, osterix and osteocalcin) was also restored by treatment with either U0126, LY294002, or PHPS1 in a dose-dependent manner, while it was enhanced by treatment with V Stattic (Fig. 5b). Moreover, a high dose of PHPS1, 20 μM, caused significantly upregulated expression of osteocalcin.

For mineralization of ECM, the negative effect of IL-6/sIL-6R was restored by treatment with either U0126, LY294002, or PHPS1. As with ALP activity and osteoblastic gene expression, the negative effect of IL-6/sIL-6R on mineralization was enhanced by treatment with V Stattic (Fig. 6a, b). ALP activity, osteoblastic gene expression, and mineralization of ECM in cells treated only with each inhibitor demonstrated the same behavior (Figs. 5, 6).

Furthermore, the negative effects of ALP activity, osteoblastic gene expression and mineralization of ECM by stimulation with IL-6/sIL-6R were compared for levels in the presence and in the absence of each inhibitor. The negative effects on osteoblast differentiation by IL-6/sIL-6R showed a tendency to decrease in the presence of each inhibitor, as compared to the absence of inhibitors (Figs. 5, 6). The negative effects were decreased by 15–44, 20–61, 7–140, and 21–80 % in the presence of U0126, LY294002, PHPS1 and V Stattic, respectively, as compared to the absence of inhibitors. These results indicate that the effects of IL-6/sIL-6R on osteoblast differentiation might be mediated either by MEK/ERK, PI3K/Akt, or JAK/STAT3 pathways.

Knockdown of MEK2 and Akt2 via siRNA transfection restores ALP activity and Runx2 gene expression

To further confirm the effects of MEK and Akt inhibition on osteoblast differentiation in MC3T3-E1 cells, we studied cell differentiation after knockdown of MEK and Akt. For each protein, RNAs of two isoforms were separately blocked: MEK1 and MEK2 for MEK, and Akt1 and Akt2 for Akt.

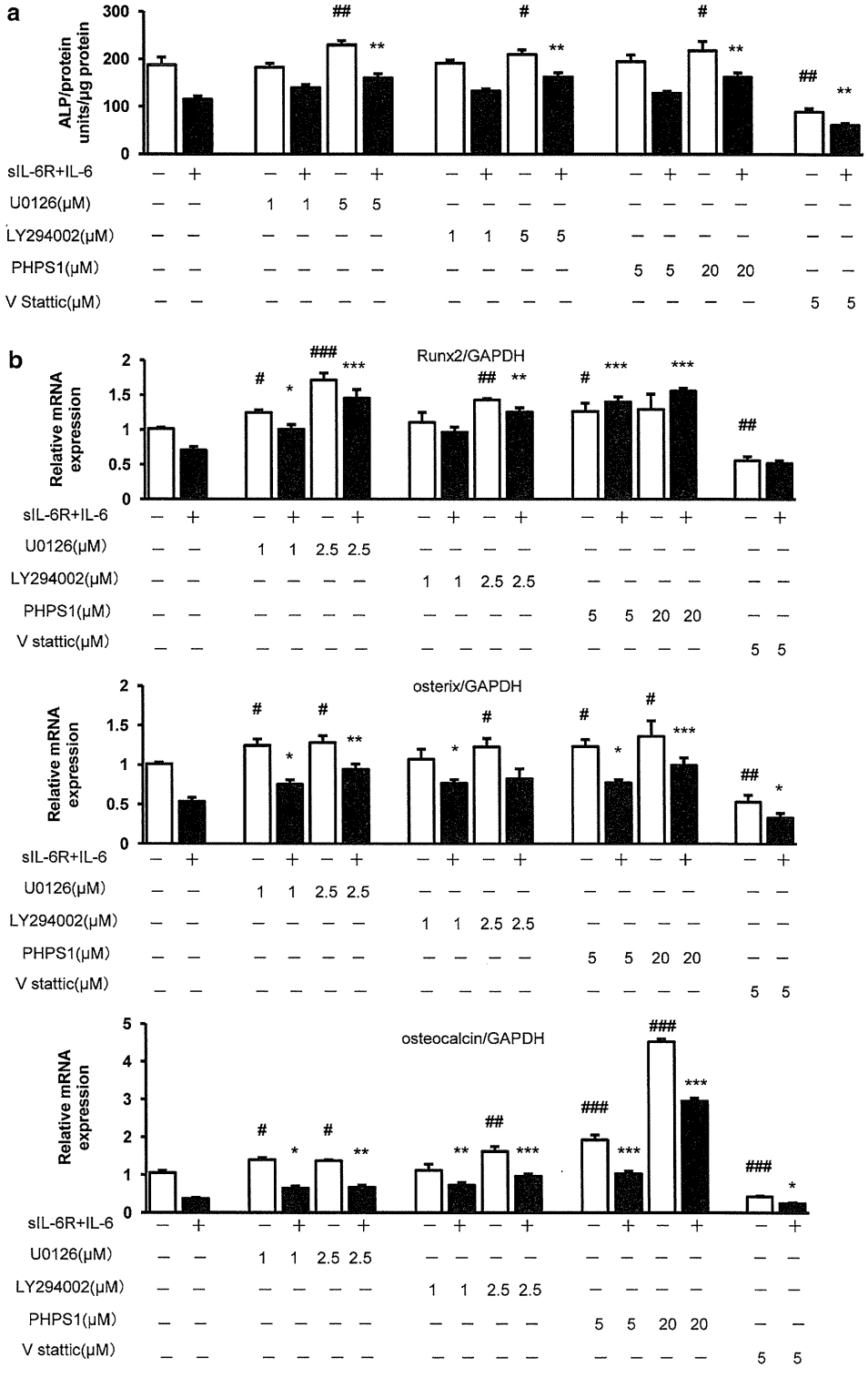

Fig. 5 The negative effects of IL-6 on ALP activity and the expression of osteoblastic genes were restored by inhibition of MEK, PI3K, and SHP2, while they were enhanced by inhibition of STAT3. MC3T3-E1 cells were pretreated either with U0126 (1, 2.5, 5 μM; 1 h), LY294002 (1, 2.5, 5 μM; 1 h), PHPS1 (5, 20 μM; 1 h), or V Stattic (5 μM; 1 h), then stimulated either with 10 ng/ml IL-6 and 100 ng/ml sIL-6R or with vehicle and incubated for 6 days. (a) ALP activity of the cell lysates was measured using p-nitrophenylphosphate as a substrate. The negative effect of IL-6 on ALP activity was restored by treatment with either U0126, LY294002, or PHPS1 in a dose-dependent manner, while it was enhanced by treatment with V Stattic. **b** Total RNA was extracted and real-time PCR for Runx2, osterix, and osteocalcin was performed. Data were normalized to GAPDH expression and are shown as the ratio of gene expression compared to control cells treated with vehicle. The negative effect of IL-6 on expression of osteoblastic genes was restored by treatment either with U0126, LY294002, or PHPS1 in a dose-dependent manner, while it was enhanced by treatment with V Stattic. Representative data from at least three independent experiments are shown. Data are shown as mean ± SE. *n.s.* not significant; $^{\#}P < 0.05$; $^{\#\#}P < 0.001$; $^{\#\#\#}P < 0.001$, compared to the group treated with vehicle. $^{*}P < 0.05$; $^{**}P < 0.001$; $^{***}P < 0.001$, compared to group treated with IL-6/sIL-6R

The protein expression level of each molecule was found to be diminished selectively at 48 h after transfection of the respective siRNAs (Fig. 7a). The ALP activity in MC3T3-E1 cells treated with IL-6/sIL-6R was restored by knockdown of MEK2 and Akt2 as compared to that in cells transfected with negative control siRNA. On the other hand, knockdown of MEK1 and Akt1 enhanced the negative effects of IL-6/sIL-6R on ALP activity (Fig. 7b) (ALP activity after transfection with each siRNA without IL-6/sIL-6R demonstrated the same behavior; Fig. 7b) Quantitative real-time PCR analysis revealed that the gene expressions of Runx2, osterix, and

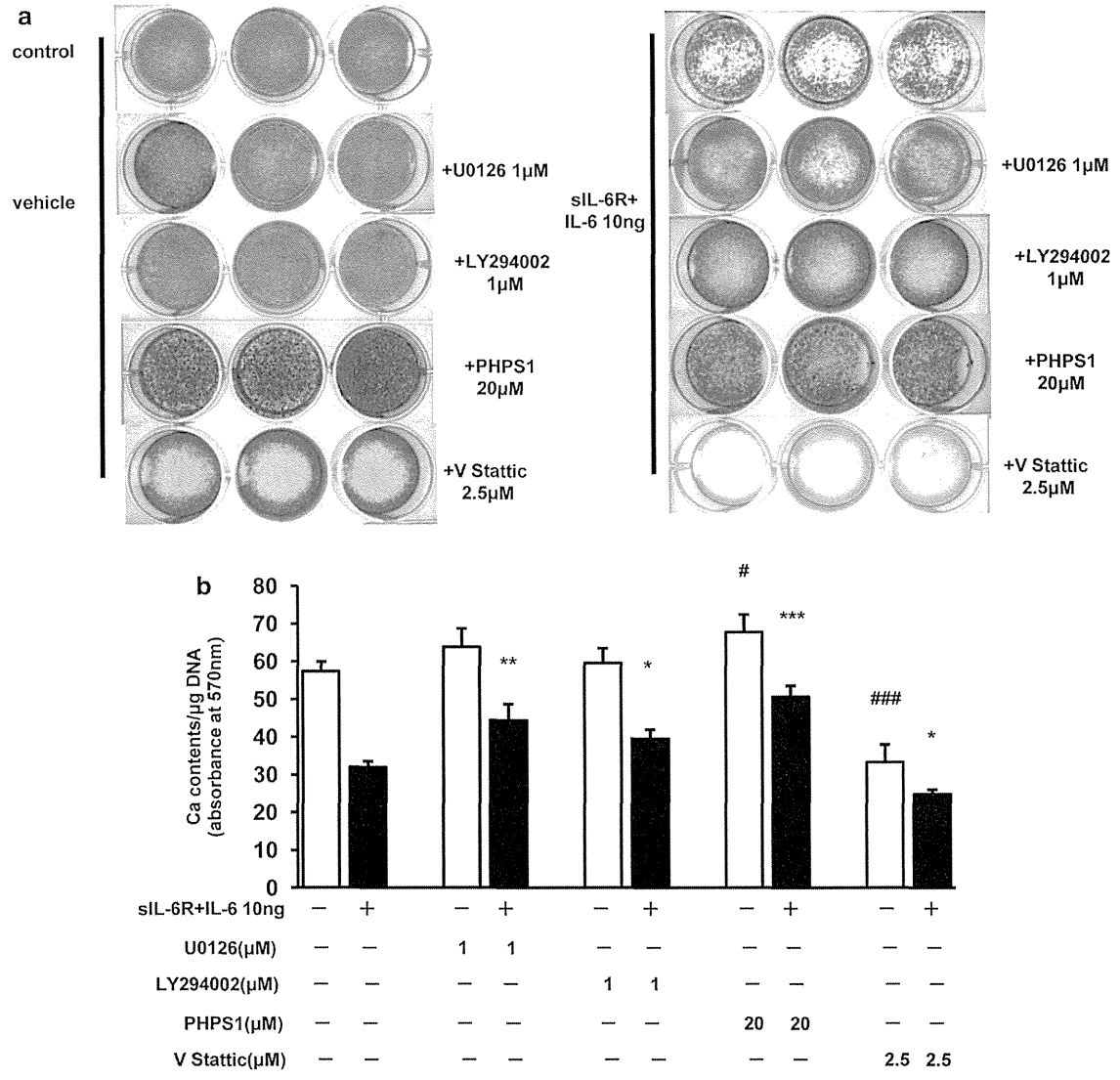

Fig. 6 The negative effect of IL-6 on mineralization of ECM was restored by inhibition of MEK, PI3K, and SHP2, while it was enhanced by inhibition of STAT3. MC3T3-E1 cell were pretreated either with U0126 (1 μM; 1 h), LY294002 (1 μM; 1 h), PHPS1 (20 μM; 1 h), or V Stattic (2.5 μM; 1 h), then stimulated with either 10 ng/ml IL-6 and 100 ng/ml sIL-6R or with vehicle and incubated for 21 days. **a** After fixation, the cells were stained with alizarin red solution. The reduction of alizarin red staining by IL-6/sIL-6R was restored in cells treated with either U0126, LY294002, or PHPS1, while it was enhanced in those treated with V Stattic. **b** Quantification of matrix mineralization was by measurement of absorbance for alizarin red normalized by total DNA content. The reduction of matrix mineralization by IL-6/sIL-6R was restored in cells treated with either U0126, LY294002, or PHPS1, while it was enhanced in those treated with V Stattic. Representative data from at least three independent experiments are shown. Data are shown as mean ± SE. *n.s.* not significant; $^{\#}P < 0.05$; $^{\#\#}P < 0.001$; $^{\#\#\#}P < 0.001$, compared to the group treated with vehicle. $^{*}P < 0.05$; $^{**}P < 0.001$; $^{***}P < 0.001$, compared to group treated with IL-6/sIL-6R

osteocalcin were restored by knockdown of MEK2. On the other hand, knockdown of Akt2 also restored Runx2, but decreased osteocalcin expression (Fig. 7c), while knockdown of Akt2 without IL-6/sIL-6R caused no significant difference in Runx2 expression (Fig. 7b). As was recognized for ALP activity, knockdown of MEK1 and Akt1 enhanced the downregulation of osteocalcin expression (Fig. 7b, c). Also, the negative effects of IL-6/sIL-6R on osteoblast differentiation showed some tendency to decrease with each knockdown compared to those without knockdown. The negative effects were decreased by 2–24, 4–27, 7–43, and 21–26 % with knockdown of MEK1, MEK2, Akt1, and Akt2, respectively, as compared to those without knockdown. These results indicate that IL-6 may suppress osteoblast differentiation through MEK2 and Akt2.

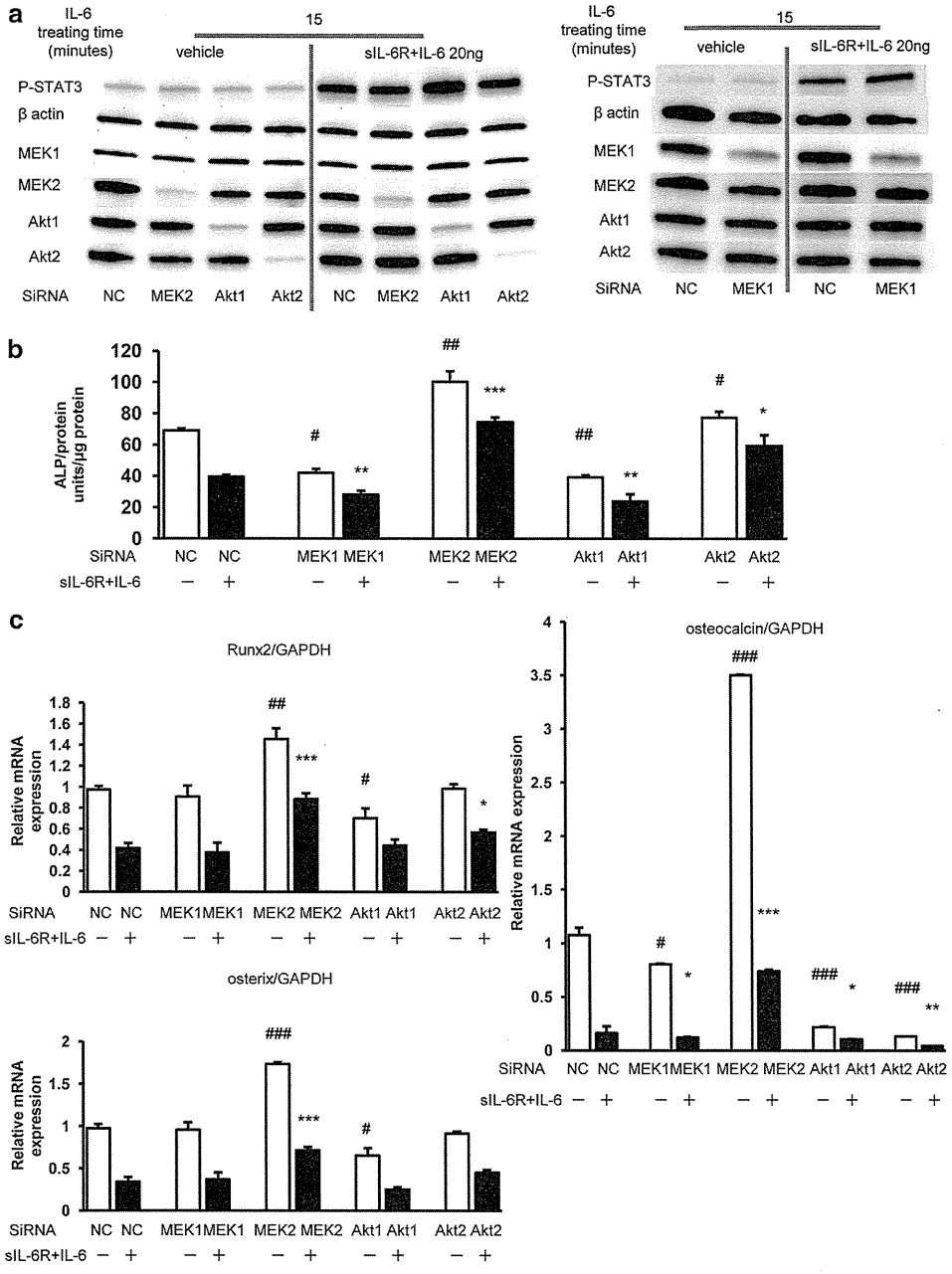

Fig. 7 Knockdown of MEK2 and Akt2 in cells transfected with siRNA restored ALP activity and Runx2 gene expression. **a** MC3T3-E1 cells transfected with respective siRNAs were cultured for 48 h. Western blotting was performed using cell lysates stimulated with vehicle or with 20 ng/ml IL-6 and 100 ng/ml sIL-6R (15 min). Expression levels of each protein, MEK1, MEK2, Akt1, and Akt2, were selectively diminished at 48 h after transfection with respective siRNAs. **b** MC3T3-E1 cells transfected with respective siRNAs were incubated for 48 h after which the medium was changed to differentiation medium with vehicle or with 20 ng/ml IL-6 and 100 ng/ml sIL-6R. The cells were then incubated for 3 days to evaluate osteoblast differentiation. ALP activity in MC3T3-E1 cells treated with IL-6/sIL-6R was restored by knockdown of MEK2 and Akt2 as compared to that in cells transfected with negative control siRNA. **c** Expression of osteoblastic genes in MC3T3-E1 cells transfected with respective siRNAs was assessed by real-time PCR. The expression of each gene was normalized against GAPDH expression. The gene expressions of Runx2, osterix, and osteocalcin were restored by knockdown of MEK2. Knockdown of Akt2 also restored Runx2, but decreased osteocalcin. Representative data from at least three independent experiments are shown. Data are shown as mean ± SE. *n.s.* not significant; $^{\#}P < 0.05$; $^{\#\#}P < 0.001$; $^{\#\#\#}P < 0.001$, compared to negative control group treated with vehicle. $^{*}P < 0.05$; $^{**}P < 0.001$; $^{***}P < 0.001$, compared to negative control group treated with IL-6/sIL-6R

IL-6/sIL-6R inhibits the differentiation of primary murine calvarial osteoblasts by activating phosphorylation of ERK, Akt2, and STAT3

Experiments were repeated with murine calvarial osteoblasts isolated from the calvariae of 3-day-old C57BL/6 mice. As was recognized in MC3T3-E1 cells, IL-6 inhibited ALP activity (Fig. 8a), the expression of osteoblastic genes (Fig. 8b), and mineralization (Fig. 8c, d) in a dose-dependent manner. Furthermore, IL-6 induced phosphorylation of ERK, Akt2, and STAT3 (Fig. 8e), which was exactly the same as with MC3T3-E1 cells.

Discussion

We examined the effects of IL-6 and its soluble receptor on the proliferation and differentiation of murine MC3T3-E1 osteoblastic cells and primary murine calvarial osteoblasts. Our results showed that they significantly reduced ALP activity, bone mineralization, and expression of the osteoblastic genes Runx2 osterix and osteocalcin, in a dose-dependent manner. From these experiments, we clearly demonstrated that IL-6 inhibited osteoblast differentiation of MC3T3-E1 cells and primary murine calvarial osteoblasts.

It has been demonstrated that the JAK/STAT3 signaling pathway has important roles both, in vivo and in vitro, in the differentiation of osteoblasts [37, 38]. Our results are consistent with previous reports and imply that the activation of STAT3 induced by IL-6 may induce osteoblast differentiation.

IL-6 activates another major intracellular signaling pathway, SHP2/ERK, and can also lead to the activation of an additional signaling cascade involving SHP2/PI3K/Akt. IL-6-induced activation of PI3K and downstream protein kinase Akt/PKB has been reported to play important roles in the proliferation of prostate cancer cells [30, 31], hepatoma cells [32], and multiple myeloma cells [29]. They were also reported to associate with neuroendocrine differentiation of prostate cancer cells induced by IL-6 [32]. In this study, we focused on the PI3K/Akt pathway triggered by IL-6, because no reports have demonstrated the role of IL-6 in the activation of PI3K/Akt signaling pathway in osteoblasts. We have demonstrated for the first time that IL-6-induced activation of Akt2, one of the downstream pathways of SHP2, may be a key player in the negative regulation of osteoblast differentiation induced by IL-6. Among the three isoforms of Akt, Akt1 and Akt2 are highly expressed in osteoblasts [39]. Mice lacking Akt1, the major isoform in bone tissue, exhibit osteopenia [40, 41], and the impact of Akt1 deficiency in osteoblast differentiation and bone development have also been published [39, 42–44], all of which are consistent with our results showing that knockdown of Akt1 signaling by siRNA inhibited osteoblast differentiation. In contrast, Mukherjee et al. [44] reported enhanced osteogenic differentiation in the absence of Akt1 in cell lines. Moreover, they reported that Akt2 was required for BMP2-initiated osteoblast differentiation of cultured murine mesenchymal stem cells, but that Akt1 was dispensable in this assay [45], which is inconsistent with our results showing that knockdown of Akt2 signaling by siRNA promoted osteoblast differentiation. These discrepancies might be due to the difference between cell types, i.e. intramembranous (calvariae) cells and endochondral (long bones) cells.

In this study, gene expression of osteocalcin, a late osteoblastic differentiation marker, was upregulated by treatment with a PI3K/Akt inhibitor, but was downregulated by knockdown of both Akt1 and Akt2. Moreover, a complete blockade with a high dose (more than 10 μM) of the PI3K/Akt inhibitor conversely downregulated the expression of osteocalcin (data not shown). This discrepancy may be due to the difference between the temporary or partial blockade by the inhibitor and constitutive knockdown by siRNA. Since bone formation has been reported to increase without impairment of mineralization and resorption even in osteocalcin-deficient mice [46], the expression of osteocalcin may not directly affect bone formation.

We have previously reported that osteoblast differentiation was significantly promoted by MEK inhibitor in BMP-2-treated C2C12 cells and MC3T3-E1 cells [47]. Our findings in the present study are consistent with our previous report and others [47–49] at the point that IL-6-induced activation of ERK significantly downregulated osteoblast differentiation. In addition, our results suggest that there might be different roles in osteoblast differentiation between MEK1 and MEK2. Constitutively active expression of MEK1 has been reported to accelerate bone development both in vitro [50] and in vivo [51], which is consistent with the results showing that knockdown of MEK1 inhibited osteoblast differentiation in the present study. As for MEK2, there are no reports concerning its roles in osteoblast differentiation, and we are the first to demonstrate that MEK2 may also be a key player in the negative regulation of osteoblast differentiation induced by IL-6. The effects of an MEK inhibitor that inhibits both MEK1 and MEK2 on bone formation are still controversial [52]. These controversies might be due to different roles played between MEK1 and MEK2 in osteoblast differentiation, and the effects of MEK inhibitors could depend on which pathway is predominantly inhibited in each study.

With respect to intracellular signaling pathways, our results showed that IL-6 triggers three signaling pathways, one of which has a conflicting function with the others.

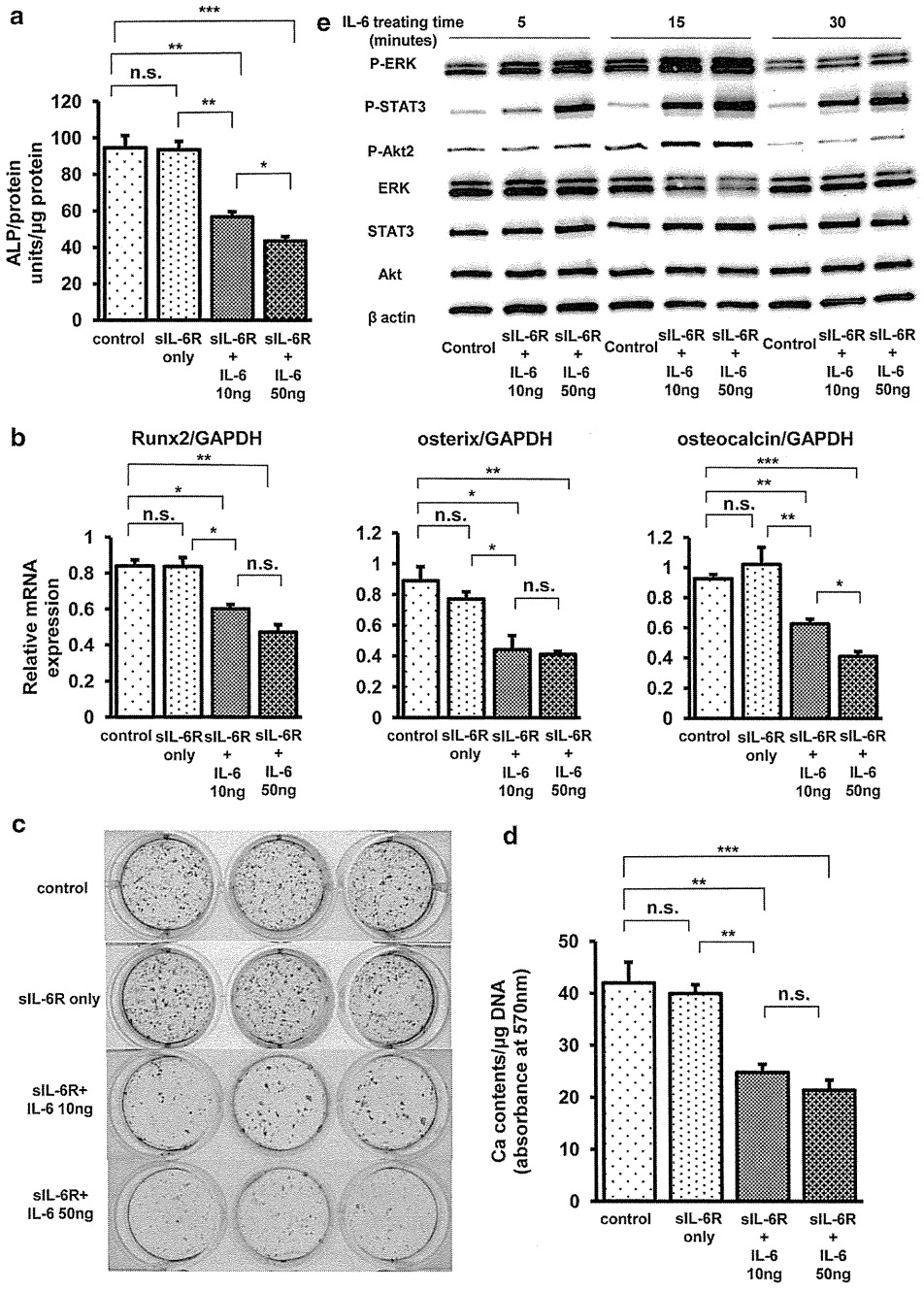

Fig. 8 IL-6/sIL-6R inhibited the differentiation of primary murine calvarial osteoblasts with the activated phosphorylation of ERK, Akt2, and STAT3. **a** ALP activity of lysates of murine calvarial osteoblasts treated with or without IL-6/sIL-6R for 6 days was measured using p-nitrophenylphosphate as a substrate. IL-6/sIL-6R significantly reduced ALP activity in a dose-dependent manner. **b** Total RNA was extracted from murine calvarial osteoblasts treated with or without IL-6/sIL-6R for 6 days, and real-time PCR for Runx2, osterix, and osteocalcin was performed. Data were normalized to GAPDH expression and are shown as the ratio of gene expression as compared to control cells treated with vehicle. The expression of osteoblastic genes was significantly downregulated by IL-6/sIL-6R in a dose-dependent manner. **c** Murine calvarial osteoblasts were treated with or without IL-6/sIL-6R and were cultured for 21 days. After fixation, the cells were stained with alizarin red solution. Apparently significant reduction of alizarin red staining was recognized in cells treated with either 10 or 50 ng/ml IL-6. **d** Matrix mineralization was quantified by measurement of absorbance for alizarin red normalized by total DNA content. IL-6/sIL-6R significantly inhibited mineralization of ECM in a dose-dependent manner. **e** Primary murine calvarial osteoblasts were treated with vehicle or 10 or 50 ng/ml IL-6 and 100 ng/ml sIL-6R in a time-course experiment (5, 15, and 30 min). Western blotting was performed using cell lysates. IL-6 significantly induced the phosphorylation of ERK, Akt2, and STAT3 in a dose-dependent manner. Representative data from at least three independent experiments are shown. Data are shown as mean ± SE. *n.s.* not significant; $*P < 0.05$; $**P < 0.001$; $***P < 0.001$

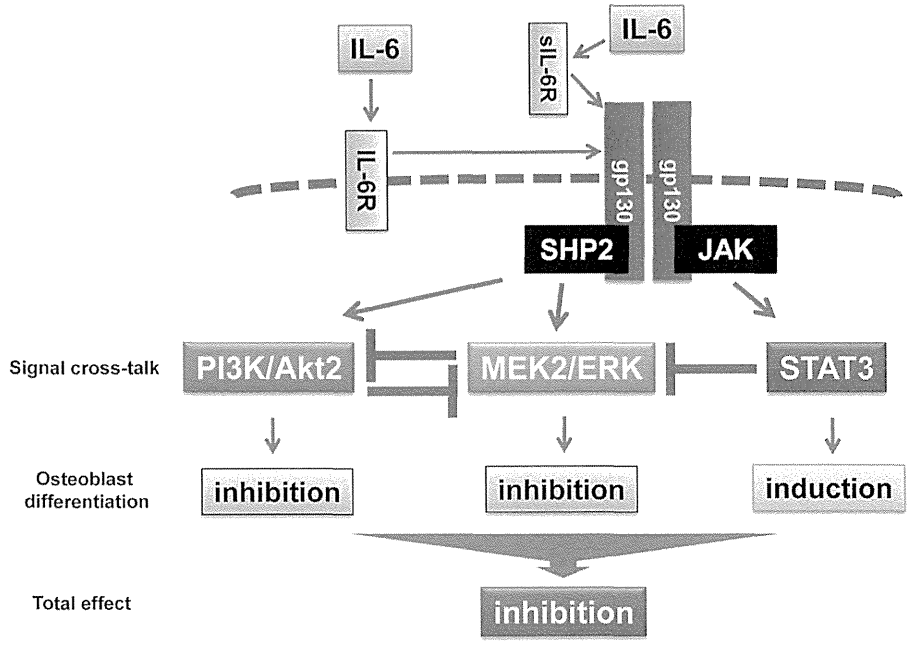

Fig. 9 Schematic presentation of signaling pathways involved in osteoblast differentiation induced by IL-6. IL-6-induced novel SHP2/MEK2/ERK and SHP2/PI3K/Akt2 signal crosstalk in osteoblastic cells; ERK and Akt signaling pathways, both of which are downstream of SHP2, negatively regulate each other reciprocally. On the other hand, the STAT3 signaling pathway negatively regulates the ERK signaling pathway. MEK2/ERK and PI3K/Akt2 have negative effects on osteoblast differentiation, whereas STAT3 has a positive effect. Overall, IL-6 inhibits osteoblast differentiation through MEK2 and Akt2 signaling pathways

SHP2/ERK and SHP2/Akt2 negatively affects osteoblast differentiation, whereas JAK/STAT3 positively affects it (Fig. 9). In other cells, it is often that simultaneous activation of the SHP2/ERK and JAK/STAT3 cascades generate opposing, or at least different signals. In osteoclasts, for example, SHP2/ERK activation inhibits osteoclastogenesis [53], whereas STAT3 is a pro-osteoclastic molecule after phosphorylation on serine727 [54]. In myeloid leukemic M1 cells, STAT3 induces differentiation in vitro [55], whereas the SHP2/ERK pathway promotes their proliferation [56]. These examples suggest that the integration of opposing activities transduced by more than one pathway could provide a biologically balanced state in the end, leaving availability to respond to another physiological situation. Indeed, Hirano and colleagues [57] have proposed a "signaling orchestration" model in a single cell, where the balance or interplay of simultaneously generated contradictory signals eventually determines the biological outcome. Thus, the inconsistent results regarding the effects of IL-6 on osteoblast differentiation in previous reports could be explained by which intracellular signaling pathway was predominantly activated in each study. The balance of three signaling pathways could be influenced by such conditions as the variety of cultured cells, the stage of cell differentiation, and the employed culture conditions.

To the best of our knowledge, this is the first report of signal crosstalk in which IL-6-induced ERK and Akt signaling pathways negatively regulated each other in cultured osteoblastic cells. In this study, however, cancellation of the negative effects of IL-6/sIL-6R on osteoblast differentiation by inhibitors was incomplete as compared to the absence of inhibitor (Figs. 5, 6). This might be because ERK, Akt and STAT3 are all critical pathways in osteoblast differentiation even in the absence of IL-6/sIL-6R, and even though one pathway is blocked, another pathway is enhanced by reciprocal regulation in the crosstalk between IL-6-activated signaling pathways (Fig. 9). Our results demonstrated that a STAT3 inhibitor significantly enhanced IL-6-induced activation of ERK and SHP2, but not of Akt (Fig. 4a). SHP2 could predominantly lead to the activation of the ERK signaling pathway as compared to Akt, and the enhanced signaling of ERK may restrain the enhancement of the Akt signaling pathway in a negative feedback manner.

The results obtained from the present study show that SHP2, MEK and PI3K inhibitors would be of potential use for the treatment of osteoporotic changes in RA patients. In particular, SHP2 inhibitors not only could inhibit the negative effect of IL-6-induced MEK/ERK and PI3K/Akt2 signaling, but also enhance the positive effect of IL-6-induced STAT3 signaling on osteoblast differentiation [37]. However, since a pro-inflammatory effect of STAT3 on synovitis has been reported [36, 58], selective inhibition of MEK2 and Akt2 signaling in osteoblasts may be more promising in order to avoid the enhancement of synovitis and consequent joint destruction.

In conclusion, our study provides new insights in the pathophysiology as well as potential treatment options for bone loss in RA, focusing on osteoblast differentiation in vitro. Our results demonstrated that IL-6 could inhibit osteoblast differentiation through MEK2/ERK and PI3K/Akt2 signaling pathways, both of which are SHP2-dependent downstream signaling pathways.

Conflict of interest All authors have no conflicts of interest.

References

1. Hashizume M, Mihara M (2011) The roles of interleukin-6 in the pathogenesis of rheumatoid arthritis. Arthritis 2011:765624
2. Ito A, Itoh Y, Sasaguri Y, Morimatsu M, Mori Y (1992) Effects of interleukin-6 on the metabolism of connective tissue components in rheumatoid synovial fibroblasts. Arthritis Rheum 35:1197–1201
3. Nishimoto N, Kishimoto T (2004) Inhibition of IL-6 for the treatment of inflammatory diseases. Curr Opin Pharmacol 4:386–391
4. De Benedetti F, Robbioni P, Massa M, Viola S, Albani S, Martini A (1992) Serum interleukin-6 levels and joint involvement in polyarticular and pauciarticular juvenile chronic arthritis. Clin Exp Rheumatol 10:493–498
5. De Benedetti F, Massa M, Pignatti P, Albani S, Novick D, Martini A (1994) Serum soluble interleukin 6 (IL-6) receptor and IL-6/soluble IL-6 receptor complex in systemic juvenile rheumatoid arthritis. J Clin Invest 93:2114–2119
6. Kotake S, Sato K, Kim KJ, Takahashi N, Udagawa N, Nakamura I, Yamaguchi A, Kishimoto T, Suda T, Kashiwazaki S (1996) Interleukin-6 and soluble interleukin-6 receptors in the synovial fluids from rheumatoid arthritis patients are responsible for osteoclast-like cell formation. J Bone Miner Res 11:88–95
7. Kwan Tat S, Padrines M, Theoleyre S, Heymann D, Fortun Y (2004) IL-6, RANKL, TNF-alpha/IL-1: interrelations in bone resorption pathophysiology. Cytokine Growth Factor Rev 15:49–60
8. Palmqvist P, Persson E, Conaway HH, Lerner UH (2002) IL-6, leukemia inhibitory factor, and oncostatin M stimulate bone resorption and regulate the expression of receptor activator of NF-kappa B ligand, osteoprotegerin, and receptor activator of NF-kappa B in mouse calvariae. J Immunol 169:3353–3362
9. Le Goff B, Blanchard F, Berthelot JM, Heymann D, Maugars Y (2010) Role for interleukin-6 in structural joint damage and systemic bone loss in rheumatoid arthritis. Joint Bone Spine 77:201–205
10. Hirano T, Matsuda T, Turner M, Miyasaka N, Buchan G, Tang B, Sato K, Shimizu M, Maini R, Feldmann M et al (1988) Excessive production of interleukin 6/B cell stimulatory factor-2 in rheumatoid arthritis. Eur J Immunol 18:1797–1801
11. Ohshima S, Saeki Y, Mima T, Sasai M, Nishioka K, Nomura S, Kopf M, Katada Y, Tanaka T, Suemura M, Kishimoto T (1998) Interleukin 6 plays a key role in the development of antigen-induced arthritis. Proc Natl Acad Sci USA 95:8222–8226
12. Dasgupta B, Corkill M, Kirkham B, Gibson T, Panayi G (1992) Serial estimation of interleukin 6 as a measure of systemic disease in rheumatoid arthritis. J Rheumatol 19:22–25
13. Poli V, Balena R, Fattori E, Markatos A, Yamamoto M, Tanaka H, Ciliberto G, Rodan GA, Costantini F (1994) Interleukin-6 deficient mice are protected from bone loss caused by estrogen depletion. EMBO J 13:1189–1196
14. Yang X, Ricciardi BF, Hernandez-Soria A, Shi Y, Pleshko Camacho N, Bostrom MP (2007) Callus mineralization and maturation are delayed during fracture healing in interleukin-6 knockout mice. Bone 41:928–936
15. Kopf M, Baumann H, Freer G, Freudenberg M, Lamers M, Kishimoto T, Zinkernagel R, Bluethmann H, Kohler G (1994) Impaired immune and acute-phase responses in interleukin-6-deficient mice. Nature 368:339–342
16. De Benedetti F, Rucci N, Del Fattore A, Peruzzi B, Paro R, Longo M, Vivarelli M, Muratori F, Berni S, Ballanti P, Ferrari S, Teti A (2006) Impaired skeletal development in interleukin-6-transgenic mice: a model for the impact of chronic inflammation on the growing skeletal system. Arthritis Rheum 54:3551–3563
17. Naka T, Nishimoto N, Kishimoto T (2002) The paradigm of IL-6: from basic science to medicine. Arthritis Res 4(Suppl 3):S233–S242
18. Wong PK, Campbell IK, Egan PJ, Ernst M, Wicks IP (2003) The role of the interleukin-6 family of cytokines in inflammatory arthritis and bone turnover. Arthritis Rheum 48:1177–1189
19. Garnero P, Thompson E, Woodworth T, Smolen JS (2010) Rapid and sustained improvement in bone and cartilage turnover markers with the anti-interleukin-6 receptor inhibitor tocilizumab plus methotrexate in rheumatoid arthritis patients with an inadequate response to methotrexate: results from a substudy of the multicenter double-blind, placebo-controlled trial of tocilizumab in inadequate responders to methotrexate alone. Arthritis Rheum 62:33–43
20. Franchimont N, Wertz S, Malaise M (2005) Interleukin-6: an osteotropic factor influencing bone formation? Bone 37:601–606
21. Li YP, Stashenko P (1992) Proinflammatory cytokines tumor necrosis factor-alpha and IL-6, but not IL-1, down-regulate the osteocalcin gene promoter. J Immunol 148:788–794
22. Peruzzi B, Cappariello A, Del Fattore A, Rucci N, De Benedetti F, Teti A (2012) c-Src and IL-6 inhibit osteoblast differentiation and integrate IGFBP5 signalling. Nat Commun 3:630
23. Hughes FJ, Howells GL (1993) Interleukin-6 inhibits bone formation in vitro. Bone Miner 21:21–28
24. Nishimura R, Moriyama K, Yasukawa K, Mundy GR, Yoneda T (1998) Combination of interleukin-6 and soluble interleukin-6 receptors induces differentiation and activation of JAK-STAT and MAP kinase pathways in MG-63 human osteoblastic cells. J Bone Miner Res 13:777–785
25. Taguchi Y, Yamamoto M, Yamate T, Lin SC, Mocharla H, DeTogni P, Nakayama N, Boyce BF, Abe E, Manolagas SC (1998) Interleukin-6-type cytokines stimulate mesenchymal progenitor differentiation toward the osteoblastic lineage. Proc Assoc Am Physicians 110:559–574
26. Ishihara K, Hirano T (2002) Molecular basis of the cell specificity of cytokine action. Biochim Biophys Acta 1592:281–296
27. Takahashi-Tezuka M, Yoshida Y, Fukada T, Ohtani T, Yamanaka Y, Nishida K, Nakajima K, Hibi M, Hirano T (1998) Gab1 acts as an adapter molecule linking the cytokine receptor gp130 to ERK mitogen-activated protein kinase. Mol Cell Biol 18:4109–4117
28. Hideshima T, Nakamura N, Chauhan D, Anderson KC (2001) Biologic sequelae of interleukin-6 induced PI3-K/Akt signaling in multiple myeloma. Oncogene 20:5991–6000
29. Tu Y, Gardner A, Lichtenstein A (2000) The phosphatidylinositol 3-kinase/AKT kinase pathway in multiple myeloma plasma cells: roles in cytokine-dependent survival and proliferative responses. Cancer Res 60:6763–6770
30. Chung TD, Yu JJ, Kong TA, Spiotto MT, Lin JM (2000) Interleukin-6 activates phosphatidylinositol-3 kinase, which inhibits apoptosis in human prostate cancer cell lines. Prostate 42:1–7
31. Qiu Y, Robinson D, Pretlow TG, Kung HJ (1998) Etk/Bmx, a tyrosine kinase with a pleckstrin-homology domain, is an effector of phosphatidylinositol 3′-kinase and is involved in interleukin 6-induced neuroendocrine differentiation of prostate cancer cells. Proc Natl Acad Sci USA 95:3644–3649
32. Chen RH, Chang MC, Su YH, Tsai YT, Kuo ML (1999) Interleukin-6 inhibits transforming growth factor-beta-induced apoptosis through the phosphatidylinositol 3-kinase/Akt and signal transducers and activators of transcription 3 pathways. J Biol Chem 274:23013–23019
33. Schmidt K, Schinke T, Haberland M, Priemel M, Schilling AF, Mueldner C, Rueger JM, Sock E, Wegner M, Amling M (2005) The high mobility group transcription factor Sox8 is a negative regulator of osteoblast differentiation. J Cell Biol 168:899–910

34. Ratisoontorn C, Seto ML, Broughton KM, Cunningham ML (2005) In vitro differentiation profile of osteoblasts derived from patients with Saethre-Chotzen syndrome. Bone 36:627–634
35. Hellmuth K, Grosskopf S, Lum CT, Wurtele M, Roder N, von Kries JP, Rosario M, Rademann J, Birchmeier W (2008) Specific inhibitors of the protein tyrosine phosphatase Shp2 identified by high-throughput docking. Proc Natl Acad Sci USA 105:7275–7280
36. Ernst M, Inglese M, Waring P, Campbell IK, Bao S, Clay FJ, Alexander WS, Wicks IP, Tarlinton DM, Novak U, Heath JK, Dunn AR (2001) Defective gp130-mediated signal transducer and activator of transcription (STAT) signaling results in degenerative joint disease, gastrointestinal ulceration, and failure of uterine implantation. J Exp Med 194:189–203
37. Itoh S, Udagawa N, Takahashi N, Yoshitake F, Narita H, Ebisu S, Ishihara K (2006) A critical role for interleukin-6 family-mediated Stat3 activation in osteoblast differentiation and bone formation. Bone 39:505–512
38. Sims NA (2004) Glycoprotein 130 regulates bone turnover and bone size by distinct downstream signaling pathways. J Clin Investig 113:379–389
39. Kawamura N, Kugimiya F, Oshima Y, Ohba S, Ikeda T et al (2007) Akt1 in osteoblasts and osteoclasts controls bone remodeling. PLoS One 2:e1058
40. Chen WS, Xu PZ, Gottlob K, Chen ML, Sokol K, Shiyanova T, Roninson I, Weng W, Suzuki R, Tobe K, Kadowaki T, Hay N (2001) Growth retardation and increased apoptosis in mice with homozygous disruption of the Akt1 gene. Genes Dev 15:2203–2208
41. Yang ZZ, Tschopp O, Hemmings-Mieszczak M, Feng J, Brodbeck D, Perentes E, Hemmings BA (2003) Protein kinase B alpha/Akt1 regulates placental development and fetal growth. J Biol Chem 278:32124–32131
42. Vandoorne K, Magland J, Plaks V, Sharir A, Zelzer E, Wehrli F, Hemmings BA, Harmelin A, Neeman M (2010) Bone vascularization and trabecular bone formation are mediated by PKB alpha/Akt1 in a gene-dosage-dependent manner: in vivo and ex vivo MRI. Magn Reson Med 64:54–64
43. Choi YH, Choi HJ, Lee KY, Oh JW (2012) Akt1 regulates phosphorylation and osteogenic activity of Dlx3. Biochem Biophys Res Commun 425:800–805
44. Mukherjee A, Rotwein P (2012) Selective signaling by Akt1 controls osteoblast differentiation and osteoblast-mediated osteoclast development. Mol Cell Biol 32:490–500
45. Mukherjee A, Wilson EM, Rotwein P (2010) Selective signaling by Akt2 promotes bone morphogenetic protein 2-mediated osteoblast differentiation. Mol Cell Biol 30:1018–1027
46. Ducy P, Desbois C, Boyce B, Pinero G, Story B, Dunstan C, Smith E, Bonadio J, Goldstein S, Gundberg C, Bradley A, Karsenty G (1996) Increased bone formation in osteocalcin-deficient mice. Nature 382:448–452
47. Higuchi C, Myoui A, Hashimoto N, Kuriyama K, Yoshioka K, Yoshikawa H, Itoh K (2002) Continuous inhibition of MAPK signaling promotes the early osteoblastic differentiation and mineralization of the extracellular matrix. J Bone Miner Res 17:1785–1794
48. Chaudhary LR, Avioli LV (2000) Extracellular-signal regulated kinase signaling pathway mediates downregulation of type I procollagen gene expression by FGF-2, PDGF-BB, and okadaic acid in osteoblastic cells. J Cell Biochem 76:354–359
49. Lin FH, Chang JB, Brigman BE (2011) Role of mitogen-activated protein kinase in osteoblast differentiation. J Orthop Res 29:204–210
50. Ge C, Xiao G, Jiang D, Franceschi RT (2007) Critical role of the extracellular signal-regulated kinase-MAPK pathway in osteoblast differentiation and skeletal development. J Cell Biol 176:709–718
51. Matsushita T, Chan YY, Kawanami A, Balmes G, Landreth GE, Murakami S (2009) Extracellular signal-regulated kinase 1 (ERK1) and ERK2 play essential roles in osteoblast differentiation and in supporting osteoclastogenesis. Mol Cell Biol 29:5843–5857
52. Schindeler A, Little DG (2006) Ras-MAPK signaling in osteogenic differentiation: friend or foe? J Bone Miner Res 21:1331–1338
53. Sims NA, Jenkins BJ, Quinn JM, Nakamura A, Glatt M, Gillespie MT, Ernst M, Martin TJ (2004) Glycoprotein 130 regulates bone turnover and bone size by distinct downstream signaling pathways. J Clin Invest 113:379–389
54. Duplomb L, Baud'huin M, Charrier C, Berreur M, Trichet V, Blanchard F, Heymann D (2008) Interleukin-6 inhibits receptor activator of nuclear factor kappaB ligand-induced osteoclastogenesis by diverting cells into the macrophage lineage: key role of Serine727 phosphorylation of signal transducer and activator of transcription 3. Endocrinology 149:3688–3697
55. Yamanaka Y, Nakajima K, Fukada T, Hibi M, Hirano T (1996) Differentiation and growth arrest signals are generated through the cytoplasmic region of gp130 that is essential for Stat3 activation. EMBO J 15:1557–1565
56. Nakajima K, Yamanaka Y, Nakae K, Kojima H, Ichiba M, Kiuchi N, Kitaoka T, Fukada T, Hibi M, Hirano T (1996) A central role for Stat3 in IL-6-induced regulation of growth and differentiation in M1 leukemia cells. EMBO J 15:3651–3658
57. Hirano T, Matsuda T, Nakajima K (1994) Signal transduction through gp130 that is shared among the receptors for the interleukin 6 related cytokine subfamily. Stem Cells 12:262–277
58. Krause A, Scaletta N, Ji JD, Ivashkiv LB (2002) Rheumatoid arthritis synoviocyte survival is dependent on Stat3. J Immunol 169:6610–6616

Biochemical and Biophysical Research Communications 454 (2014) 12–18

Contents lists available at ScienceDirect

Biochemical and Biophysical Research Communications

journal homepage: www.elsevier.com/locate/ybbrc

Cyp26b1 within the growth plate regulates bone growth in juvenile mice

Yoshiki Minegishi [a,b,c], Yasuo Sakai [c,d], Yasuhito Yahara [a], Haruhiko Akiyama [e], Hideki Yoshikawa [f], Ko Hosokawa [c], Noriyuki Tsumaki [a,g,*]

[a] Department of Cell Growth and Differentiation, Center for iPS Cell Research and Application, Kyoto University, 53 Kawahara-cho, Shogoin, Sakyo-ku, Kyoto 606-8507, Japan
[b] Department of Plastic and Reconstructive Surgery, University of Fukui Hospital, 23-3 Matsuokashimoaizuki, Eiheiji-cho, Yoshida-gun, Fukui 910-1193, Japan
[c] Department of Plastic Surgery, Osaka University Graduate School of Medicine, 2-2 Yamadaoka, Suita, Osaka 565-0871, Japan
[d] Department of Plastic Surgery, Bellland General Hospital, 500-3 Higashiyama Naka-ku, Sakai, Osaka 599-8247, Japan
[e] Department of Orthopaedic Surgery, Gifu University Graduate School of Medicine, 1-1 Yanagito, Gifu 501-1194, Japan
[f] Department of Orthopaedic Surgery, Osaka University Graduate School of Medicine, 2-2 Yamadaoka, Suita, Osaka 565-0871, Japan
[g] Japan Science and Technology Agency, CREST, Tokyo 102-0075, Japan

ARTICLE INFO

Article history:
Received 20 September 2014
Available online 8 October 2014

Keywords:
Retinoic acid
Growth plate
Cyp26b1
Chondrocytes

ABSTRACT

Retinoic acid (RA) is an active metabolite of vitamin A and plays important roles in embryonic development. CYP26 enzymes degrade RA and have specific expression patterns that produce a RA gradient, which regulates the patterning of various structures in the embryo. However, it has not been addressed whether a RA gradient also exists and functions in organs after birth. We found localized RA activities in the diaphyseal portion of the growth plate cartilage were associated with the specific expression of *Cyp26b1* in the epiphyseal portion in juvenile mice. To disturb the distribution of RA, we generated mice lacking *Cyp26b1* specifically in chondrocytes (*Cyp26b1*$^{\Delta chon}$ cKO). These mice showed reduced skeletal growth in the juvenile stage. Additionally, their growth plate cartilage showed decreased proliferation rates of proliferative chondrocytes, which was associated with a reduced height in the zone of proliferative chondrocytes, and closed focally by four weeks of age, while wild-type mouse growth plates never closed. Feeding the *Cyp26b1* cKO mice a vitamin A-deficient diet partially reversed these abnormalities of the growth plate cartilage. These results collectively suggest that Cyp26b1 in the growth plate regulates the proliferation rates of chondrocytes and is responsible for the normal function of the growth plate and growing bones in juvenile mice, probably by limiting the RA distribution in the growth plate proliferating zone.

1. Introduction

Retinoic acid (RA) is an active metabolite of vitamin A and plays important roles in embryonic development. The concentration of RA is controlled by the balance between its synthesis by retinaldehyde dehydrogenase (RALDH) and its degradation by CYP26 enzymes. CYP26s are a group of P450 enzymes that metabolize RA to inactive forms [1–3]. Both RALDH and Cyp26 have specific expression patterns and produce a RA gradient [4]. This RA gradient regulates the patterning of the anterior–posterior axis of various structures, including the hindbrain and paraxial mesoderm [5]. The RA gradient also regulates the proximodistal patterning and outgrowth of the developing limbs. *Cyp26b1* is expressed in the distal region of developing limb buds, and mice that lack *Cyp26b1* show severe limb malformation due to the spreading of the RA signal toward the distal end of the developing limb, causing abnormal patterning of limb skeletal elements [6]. However, whether this RA gradient also regulates the growth and maintenance of organs after birth has not been addressed.

The growth plate cartilage is where bone growth occurs in juveniles. Growth plate cartilage is located in the metaphysis at each end of long bones. Chondrocytes residing at the epiphyseal side in the growth plate cartilage proliferate and subsequently undergo hypertrophy just after stopping proliferation. As a result, chondrocytes change from proliferating chondrocytes on the

Abbreviations: RA, retinoic acid; *RARE*, RA-responsive elements; *Cyp26b1*$^{\Delta chon}$ cKO, *11Enh-Cre Cyp26b1*$^{flox/flox}$ conditional knockout.

* Corresponding author at: Department of Cell Growth and Differentiation, Center for iPS Cell Research and Application, Kyoto University, 53 Kawahara-cho, Shogoin, Sakyo-ku, Kyoto 606-8507, Japan. Fax: +81 75 366 7047.
E-mail address: ntsumaki@cira.kyoto-u.ac.jp (N. Tsumaki).

http://dx.doi.org/10.1016/j.bbrc.2014.10.001
0006-291X/

epiphyseal side to hypertrophic chondrocytes on the diaphyseal side of growth plate cartilage. The hypertrophic chondrocytes residing at the diaphyseal end of the growth plate cartilage subsequently die, and the hypertrophic cartilage is degraded and gradually replaced by bone. Through this mechanism, the bone becomes elongated. Thus, strict regulation of chondrocyte proliferation and hypertrophic differentiation is necessary for the normal growth of bones.

In juveniles, focal closures of the growth plate in the distal tibia [7], the proximal tibia [8], the distal tibia, elbow, proximal femur and distal femur [9] are caused by the treatment of acne with retinoids [7] or the treatment of hyperkeratinosis with cis-retinoic acid [8,9]. In guinea pigs, the application of RA caused closure of the growth plates in the proximal tibia [10]. These clinical and preclinical manifestations indicate that vitamin A and its metabolites play important roles in the bone growth of juveniles. The RA signal has been shown to regulate bone growth after birth. The deletion of RA receptors (RAR) in chondrocytes disturbs skeletal growth due to abnormal chondrocyte differentiation and disturbed matrix synthesis within the growth plates in mice [11]. Additionally, a localized distribution of RA was detected in the growth plate cartilage of the ribs of three-week-old rabbits [12]. However, it remains to be determined how RA regulates the bone growth of juveniles. In this study, we found that the expression of Cyp26b1 specifically in the proliferative chondrocyte zone was associated with localized RA activities in the zone of hypertrophic chondrocytes in the growth plate cartilage of juvenile mice. To disturb the distribution of RA, we inactivated Cyp26b1 in the growth plate using Cyp26b1 conditional knock-out mice. The resulting mouse phenotype suggests that Cyp26b1 within the growth plate regulates the proliferation rates of chondrocytes and bone growth in juveniles.

2. Materials and methods

2.1. Animals and PCR genotyping procedures

RARE-LacZ mice were a gift from Dr. Janet Rossant [13]. To generate *Cyp26b1* conditional knockout mice, *11Enh-Cre* transgenic mice [14,15] and *Cyp26b1*$^{flox/flox}$ mice [16] were prepared and mated to generate *11Enh-Cre; Cyp26b1*$^{flox/+}$ mice. Then, the *11Enh-Cre; Cyp26b1*$^{flox/+}$ and *Cyp26b1*$^{flox/flox}$ mice were intercrossed, and the *11Enh-Cre; Cyp26b1*$^{flox/flox}$ mice were considered conditional knockout (*Cyp26b1*$^{\Delta chon}$ cKO) mice. The *11Enh-Cre; Cyp26b1*$^{flox/+}$ mice were used as controls.

For genotyping, genomic DNA was isolated from the tail tips or embryonic skin and subjected to PCR analysis, according to a previously described method for the *Cre* transgene [14] and *Cyp26b1* allele [16].

2.2. Frozen sectioning and laser capture microdissection (LMD)

Mouse hindlimbs were harvested without fixation and were immediately embedded in SCEM compound (SECTION-LAB, Hiroshima, Japan). Frozen sections were prepared at 6-μm thickness with a Cryofilm type 2c(9) (SECTION-LAB) using a CM3050S cryomicrotome (Leica), according to the method described by Kawamoto [17]. The sections were briefly fixed with 100% ethanol. Semiserial sections were then stained with hematoxylin and eosin.

For LMD, frozen sections were prepared with LMD film (SECTION-LAB) using a cryomicrotome. The sections were freeze-dried in the cryostat chamber at −25 °C for one hour and briefly fixed with 100% ethanol. The proliferative zone and hypertrophic zone in the growth plate were individually captured and microdissected from cryosections using a Leica LMD7000 device (Leica) and put onto the dip of the lid of 0.5 ml tubes with cold TRIzol (Life Technologies, Tokyo, Japan).

2.3. Real-time RT-PCR

RNA was extracted from the collected samples using RNeasy Mini Kits (Qiagen, Tokyo, Japan). The total RNA was digested with DNase to eliminate any contaminating genomic DNA. For real-time quantitative RT-PCR analyses, 1 μg of total RNA was reverse-transcribed into first-strand cDNA using ReverTra Ace (Toyobo, Osaka, Japan) and random primers. The PCR amplification was performed in a reaction volume of 20 μl containing 2 μl of cDNA, 10 μl of SYBR FAST qPCR Master Mix (Kapa Biosystems, Tokyo, Japan) and 7900HT (Applied Biosystems). The RNA expression levels were normalized to the level of *Gapdh* expression. The primers used are listed in Table 1.

2.4. Staining of the skeleton

Mouse limbs were dissected, fixed in 100% ethanol overnight and then stained with Alcian blue, followed by Alizarin red S solution, according to standard protocols [18].

2.5. Histological analysis

Mouse limbs were dissected, fixed in 4% paraformaldehyde, processed and embedded in paraffin. For the immunohistochemical analysis, sections were incubated with an anti-CYP26B1 antibody (Scrum Inc., Tokyo, Japan) and an anti-type X collagen antibody (COSMO BIO CO., Ltd., Tokyo, Japan). Immune complexes were detected using secondary antibodies conjugated to Alexa Fluor 555 and Alexa Fluor 546, respectively.

2.6. BrdU staining

Mice were intraperitoneally injected with BrdU labeling reagent (10 μl/g body weight) (Zymed Laboratories Inc., South San Francisco, CA) two hours before being sacrificed. The mice were then dissected and sectioned. The incorporated BrdU was detected using a BrdU staining kit (Zymed Laboratories, Inc., South San Francisco, CA) to distinguish actively proliferating cells. The mean number of BrdU-positive cells/total cells ± standard deviation (S.D.) was calculated.

2.7. Microscope

Images were acquired on an inverted microscope (Eclipse Ti; Nikon) equipped with cameras (DS-Fi1; Nikon and C4742-80-12AG; Hamamatsu photonics) and the NIS Elements software program (Nikon).

Table 1
Primer sequences used in this study.

Primer	Sequence (5′–3′)
Col2a1 S	TTGAGACAGCACGACGTGGAG
Col2a1 AS	AGCCAGGTTGCCATCGCCATA
Col10a1 S	GGTGTGAATGGGCGGAAAG
Col10a1 AS	GCTTCCCAATACCTTCTCGTC
MMP13 S	TGTTTGCAGAGCACTACTTGAA
MMP13 AS	CAGTCACCTCTAAGCCAAAGAAA
Runx2 S	CCGCACGACAACCGCACCAT
Runx2 AS	CGCTCCGGCCCACAAATCTC
Beta galactosidase S	CTCAAACTGGCAGATGCACGGT
Beta galactosidase AS	CGTTGCACCACAGATGAAACGC
Cyp26b1 S	GCAAGATCCTACTGGGCGAAC
Cp26b1 AS	TTGGGCAGGTAGCTCTCAAGT
Gapdh S	AAGCCCATCACCATCTTCCAGGAG
Gapdh AS	ATGAGCCCTTCCACAATGCCAAAG

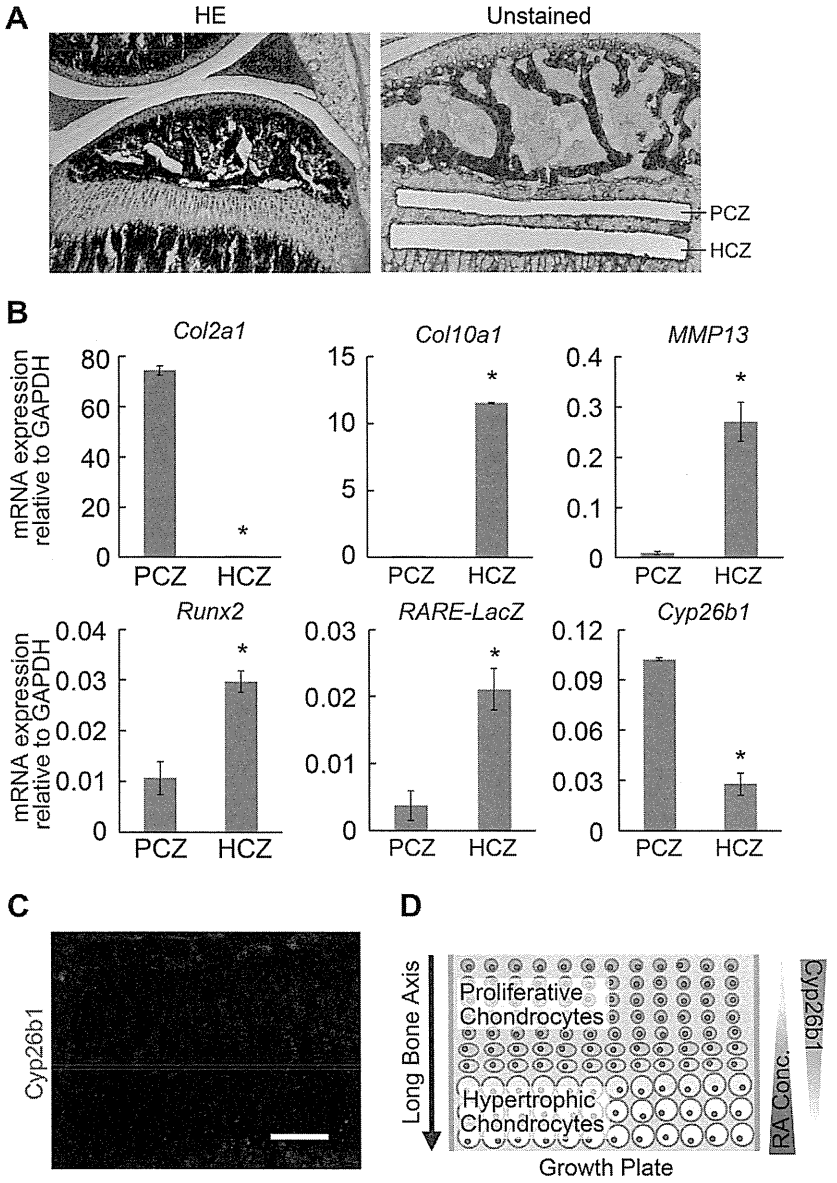

Fig. 1. Regulated RA distribution along the long axis of long bones within the growth plate cartilage. (A) We microdissected the growth plate cartilage of the proximal tibia to obtain chondrocytes from the proliferative zone (PCZ) and hypertrophic zone (HCZ) from *RARE-LacZ* mice at 2.5 weeks after birth. *Left*, a semiserial section was stained with hematoxylin and eosin. *Right*, a residual section after microdissection. (B) RNAs were extracted from cells in the proliferative chondrocyte zone (PCZ) and cells in the hypertrophic chondrocyte zone (HCZ), which were respectively obtained by microdissection, and were subjected to a real-time RT-PCR expression analysis for the genes indicated at the top of each graph. $^*P < 0.01$ ($n = 5$). (C) Histological sections of growth plate cartilage from the proximal tibias from three-week-old mice were immunostained with an anti-CYP26B1 antibody (Red). Bar: 100 μm. (D) A schematic representation of the RA concentration and *Cyp26b1* expression within the growth plate cartilage. Regulated RA activities were found along the long axis of the long bone within the growth plate cartilage and attributed to the localized expression of CYP26B1 in the proliferative chondrocyte zone.

2.8. Statistical analyses

Data are shown as the means and S.D. Student's *t*-test was used to compare data. *P* values <0.05 were considered statistically significant.

3. Results

3.1. Localized expression of Cyp26b1 and regulation of RA activities along the direction of bone elongation within the growth plate cartilage

To test our hypothesis that a RA gradient exists within the growth plate cartilage, we employed *RARE-lacZ* transgenic mice, in which *lacZ* is expressed under the control of RA-responsive elements (*RARE*) [13]. Because trabecular bone shows high background galactosidase activities, it is difficult to detect transgene-specific lacZ activities in bone, especially after birth. Therefore, we microdissected the growth plate cartilage, obtained cells from the proliferative chondrocyte and hypertrophic zones (Fig. 1A), and subjected them to an analysis of the expression of the *lacZ* transgene mRNA by real-time RT-PCR. The expression analysis of proliferative and hypertrophic chondrocyte markers confirmed that cells were isolated appropriately by microdissection (Fig. 1B). *LacZ* was much more highly expressed in the hypertrophic chondrocytes than in the proliferative chondrocytes (Fig. 1B). Interestingly, we detected a much higher level of *Cyp26b1* mRNA expression in the proliferative chondrocytes than in the

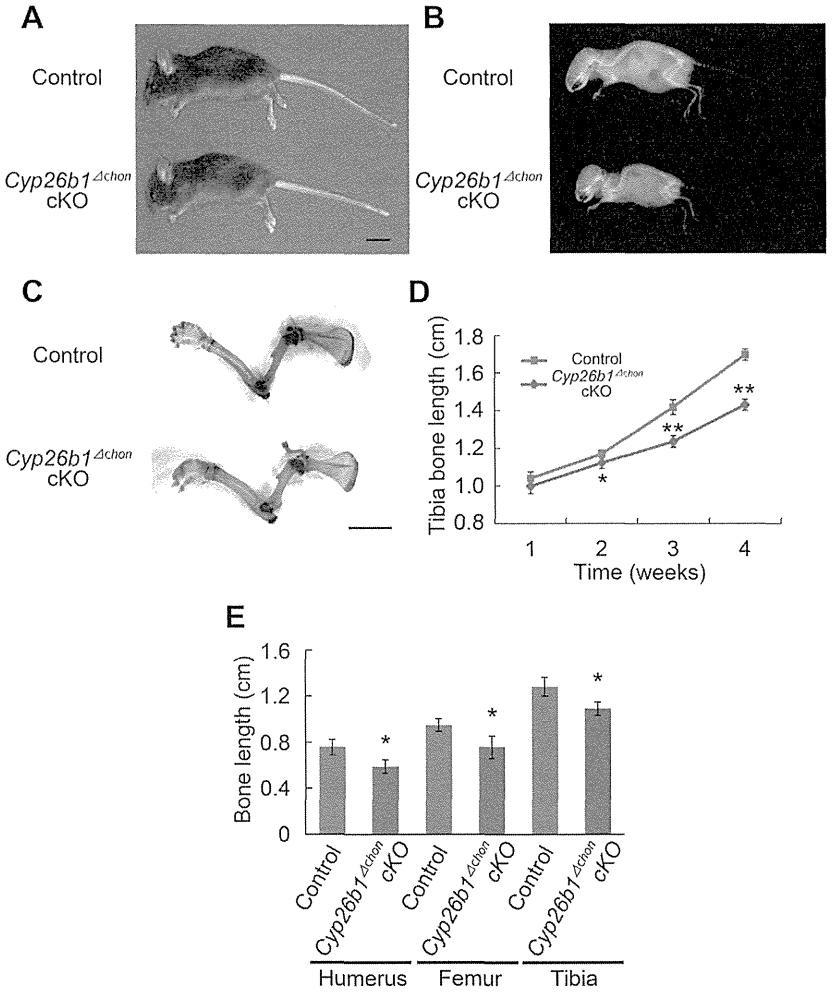

Fig. 2. The skeletal phenotype of *11Enh-Cre; Cyp26b1*$^{flox/flox}$ (*Cyp26b1*$^{\Delta chon}$) cKO mice and *11Enh-Cre; Cyp26b1*$^{flox/+}$ control mice. (A) The gross appearances of mice three weeks after birth. *Cyp26b1*$^{\Delta chon}$ cKO mice exhibited dwarfism with a short snout. Bar: 1 cm. (B) X-ray images of mice three weeks after birth. (C) The skeletons of the forelimbs of mice three weeks after birth. Alcian blue/Alizarin red staining. Bar: 5 mm. (D) The lengths of the tibiae at one, two, three and four weeks after birth. $^{*}P < 0.05$; $^{**}P < 0.01$ ($n = 5$). (E) Lengths of the humeri, femurs and tibiae three weeks after birth. $^{*}P < 0.01$ ($n = 5$).

hypertrophic chondrocytes (Fig. 1B). Accordingly, immunohistochemical analysis showed that CYP26B1 was expressed more abundantly in proliferative chondrocytes than in hypertrophic chondrocytes (Fig. 1C). These results suggest that regulated RA distribution along the direction of the bone elongation exists within the growth plate cartilage and is generated by the exclusive localization of CYP26B1 in the proliferative chondrocyte zone (Fig. 1D).

3.2. *Cyp26b1* deletion in chondrocytes disturbs the bone growth in juveniles

To disturb the distribution of RA, we deleted *Cyp26b1* in the proliferative chondrocytes of the growth plate cartilage by generating *11Enh-Cre; Cyp26b1*$^{flox/flox}$ conditional knockout (*Cyp26b1*$^{\Delta chon}$ cKO) mice. The *11Enh-Cre* transgene directed Cre expression in the proliferative chondrocytes after the completion of skeletal patterning under the control of the promoter/enhancer sequence of the type XI collagen α2 chain gene (*Col11a2*) [14,15]. *Cyp26b1*$^{\Delta chon}$ cKO mice showed normal skeletal patterning, skeletal development and bone length until one week after birth. However, at three weeks after birth, they started to show a chondrodysplasia phenotype that included dwarfism and a short snout (Fig. 2A and B). A precise examination of the lengths of skeletal elements revealed a gradual decrease in the lengths of bones compared to control mice beginning from two weeks after birth (Fig. 2C–E), and all long bones in the *Cyp26b1*$^{\Delta chon}$ cKO mice were shorter than those in the controls at three weeks after birth.

To analyze the mechanism responsible for the shorter bones in the *Cyp26b1*$^{\Delta chon}$ cKO mice, we performed a histological analysis of their growth plates. We noticed a slight decrease in the height of the proliferative chondrocyte zone at two weeks after birth (Fig. 3A, top row). The height of the proliferative chondrocyte zone was significantly decreased at three weeks after birth, especially at the central portion (Fig. 3A, middle row, and Fig. 3B). Immunohistochemistry using an anti-type X collagen antibody revealed that the location of the hypertrophic cartilage zone that produced type X collagen was shifted toward the epiphysis in Cyp26b1 cKO mice, clarifying the decreased height of the zone of proliferative chondrocytes (Fig. 3C) to the central portion.

The growth plate was closed at the central portion at four weeks after birth (Fig. 3A, bottom row), and growth plate closure was recognized in all bones examined, including the tibia, humerus and femur (Fig. 3A and D). BrdU labeling analysis revealed significantly decreased proliferation rates of the proliferative chondrocytes when the mice were one and three weeks old (Fig. 4A–C). These results suggest that the decreased proliferation rates of the

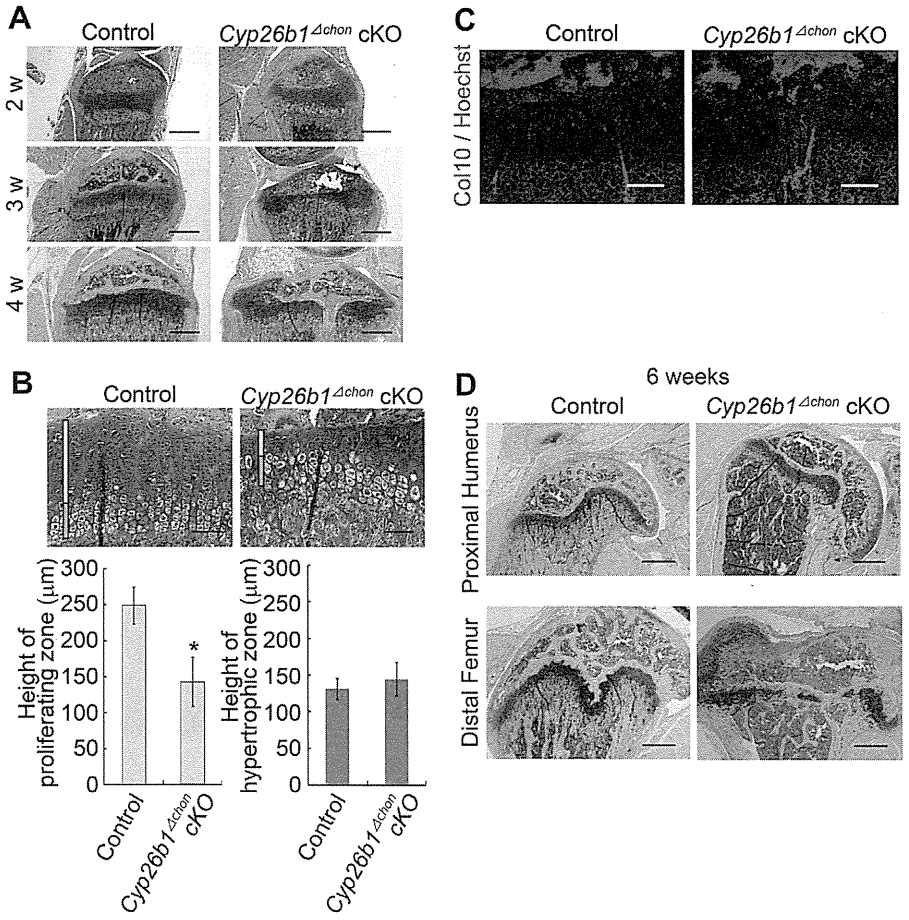

Fig. 3. Histological analysis of the growth plate cartilage of *Cyp26b1*$^{\Delta chon}$ cKO mice. (A) Sagittal sections of the proximal tibia at two, three and four weeks after birth. Safranin O-fast green-iron hematoxylin staining. Bar: 500 μm. (B) *Top*, Magnified image of the central part of the growth plate cartilage in the proximal tibia three weeks after birth. Safranin O-fast green-iron hematoxylin staining. Yellow bars indicate the height of the proliferative chondrocyte zone. Blue bars denote the height of the hypertrophic chondrocyte zone. Bars: 100 μm. Bottom, the mean ± S.D. of the height of the proliferative chondrocyte zone (left) and the hypertrophic chondrocyte zone (right). *$P < 0.01$ ($n = 5$). (C) Sagittal sections of the proximal tibia at three weeks after birth were immunostained with an anti-type X collagen antibody. Bars: 100 μm. (D) Histology of the growth plate cartilage in the proximal humerus and distal femur in *Cyp26b1*$^{\Delta chon}$ cKO mice six weeks after birth. Safranin O-fast green-iron hematoxylin. Bars: 500 μm.

proliferative chondrocytes can explain the decreased heights of the proliferative chondrocyte zone, the subsequent closure of the growth plates and the suppression of bone growth.

3.3. Reversion of the growth plate abnormalities by feeding Cyp26b1$^{\Delta chon}$ *cKO mice a vitamin A-deficient diet*

The immunohistochemical analysis confirmed that CYP26B1 was absent in the proliferative chondrocytes of *Cyp26b1*$^{\Delta chon}$ cKO mice (Fig. 4D), and that this absence could cause a disturbance in the RA distribution within the growth plate.

To confirm that the elevated concentration of RA in the proliferative chondrocytes of *Cyp26b1*$^{\Delta chon}$ cKO mice was responsible for the decreased proliferation rates, we fed the mice a vitamin A-deficient diet which systemically decreased RA concentrations [19]. Following this diet, *Cyp26b1*$^{\Delta chon}$ cKO mice showed a partial reversion in the decreased proliferation rates of the proliferative chondrocytes (Fig. 4E) and corresponding partial reversion in the decreased height of the proliferative chondrocyte zone (Fig. 4F). These results collectively suggest that the distribution of RA, which is generated by the proliferative chondrocyte-specific expression of *Cyp26b1*, regulates the proliferation rates of chondrocytes and subsequently controls the growth rates and closure of growth plates to determine the length of bones in juveniles.

4. Discussion

It is well known that the RA gradient regulates the patterning of spatial structures in mammals during development. Cyp26b1 is a critical regulator of the distribution of RA, and Cyp26b1 KO and cKO studies have demonstrated that Cyp26b1 deletion alters the RA distribution in various tissues [5,16,20,21]. The present study provides evidence that Cyp26b1 within the growth plate cartilage is important for normal chondrocyte proliferation/differentiation and bone growth in juvenile mice, probably through its regulation of the RA distribution in the growth plate.

We detected localized RA activities within the growth plate cartilage in juvenile mice, as indicated by the increased *RARE-lacZ* expression toward hypertrophic chondrocytes (Fig. 1B). The existence of a possible RA gradient within the growth plate is supported by a previous report demonstrating that the RA content measured by MS quantification was lower in the resting and proliferative chondrocyte zone than that in the hypertrophic chondrocyte zone in the growth plate cartilage of the ribs of three-week old rabbits [12]. It was reported that *RARE-lacZ* expression is not

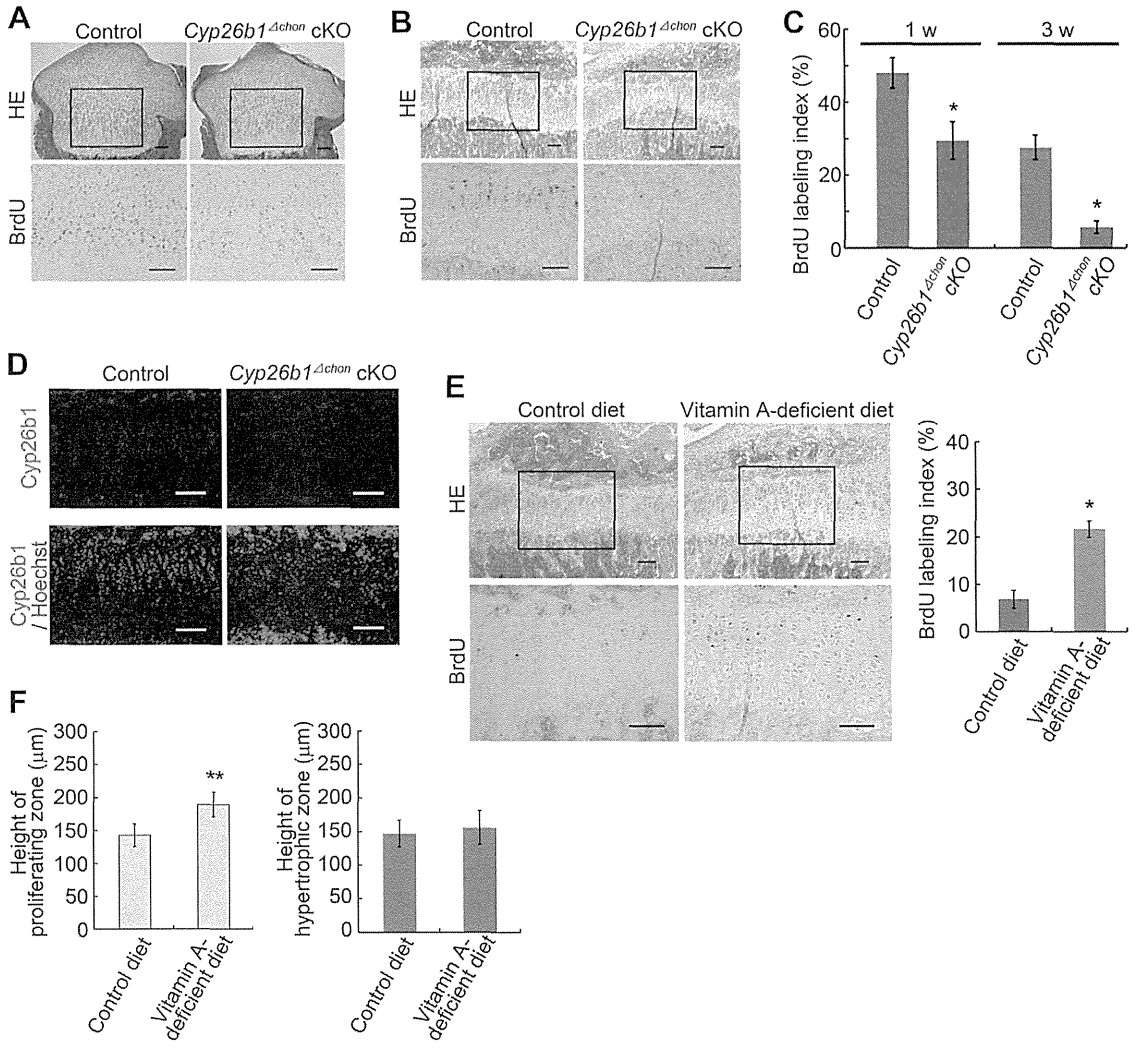

Fig. 4. Proliferation rates and Cyp26b1 expression of chondrocytes in the growth plate cartilage, and the effects of a vitamin A-deficient diet on the growth plate cartilage in the proximal tibias of *Cyp26b1*$^{\Delta chon}$ cKO mice. (A, B, C) BrdU was injected intraperitoneally into the mice two hours before sacrifice. One-week old mice (A) and three-week old mice (B). Top, hematoxylin–eosin staining. Bottom, semiserial sections were immunostained with an anti-BrdU antibody. Regions corresponding to the boxed regions in the top are magnified and shown. Bars: 100 μm. (C) Ratios (%) of the number of BrdU-positive cells to the numbers of total cells in the proliferative chondrocyte zone. $^{*}P < 0.01$ ($n = 5$). (D) Histological sections of the growth plate cartilage in the proximal tibias of three-week-old mice were immunostained with an anti-Cyp26b1 antibody (Red). The blue color is Hoechst stain, which indicates nuclei. Bars: 100 μm. (E, F) Effects of a vitamin A-deficient diet on the growth plate cartilage of *Cyp26b1*$^{\Delta chon}$ cKO mice. The mothers of *Cyp26b1*$^{\Delta chon}$ cKO pups were fed with a vitamin A-deficient diet or a control diet from eight weeks before gestation until the sacrifice of the *Cyp26b1*$^{\Delta chon}$ cKO pups three weeks after birth. The pups consumed either their mother's milk or shared an identical diet with their mother. (E) *Left*, BrdU was injected intraperitoneally into the mice two hours before sacrifice. Top, hematoxylin–eosin staining. Bottom, semiserial sections were immunostained with an anti-BrdU antibody. Regions corresponding to the boxed regions in the top are magnified and shown. Bars: 100 μm. *Right*, ratios (%) of the number of BrdU-positive cells to the number of total cells in the proliferative chondrocyte zone. $^{*}P < 0.01$ ($n = 5$). (F) Mean ± S.D. of the height of the proliferative chondrocyte zone (left) and the hypertrophic chondrocyte zone (right). $^{**}P < 0.05$ ($n = 5$).

detectable or is limited in the primordial cartilage during the embryonic stage [22], which is consistent with the normal embryonic development of *Cyp26b1*$^{\Delta chon}$ cKO mice in this study.

The partial recovery of growth plate abnormalities in *Cyp26b1*$^{\Delta chon}$ cKO mice by a vitamin A-deficient diet supports the notion that *Cyp26b1* deletion caused abnormalities through elevated RA activities in the growth plate. Accordingly, the decreased proliferation rates of proliferative chondrocytes in *Cyp26b1*$^{\Delta chon}$ cKO mice suggest that excess RA inhibits the proliferation of proliferative chondrocytes. Previous studies on the effects of RA have yielded conflicting data regarding its regulation of the differentiation of chondrocytes in the growth plate [23]. Ballock et al. reported that RA blocks the stimulatory effects of thyroid hormone on cultured rat chondrocyte hypertrophy [23], whereas others showed RA induces the hypertrophy of cultured chick chondrocytes [24,25]. Such in vitro culture experiments are affected by the pharmacological dosage of RA, variations in the species, culture conditions, composition of serum and the anatomical source of the growth plate cells used [23]. Our in vivo results are less susceptible to the above problems to better clarify the function of RA in chondrocyte proliferation/differentiation in the growth plate and in the bone growth.

Excess intake of vitamin A causes growth impairment and skeletal pain in juveniles [7–9]. Our study provides evidence that regulation of the RA distribution occurs within the growth plate cartilage and that this regulation plays critical roles in controlling the growth of long bones in juvenile mice. Our results also show that exogenous vitamin A can affect this regulation and distribution, since a vitamin A-deficient diet partially rescued the growth plate structure of *Cyp26b1*$^{\Delta chon}$ cKO mice. The characteristics of the closure of the growth plate seen in a child receiving excess RA [8] and guinea pigs receiving a RAR agonist [10] were similar

to those seen in *Cyp26b1*$^{\Delta chon}$ cKO mice in that the closure occurred in the central part of the growth plate, suggesting that a similar form of regulation occurs in humans and mice.

Acknowledgments

We thank Hiroshi Hamada and Satoru Mamiya for the *Cyp26b1* flox mice, Aki Takimoto, Chisa Shukunami and Yuji Hiraki for instructions about the cryostat sectioning, Janet Rossant for the RARE-LacZ mice, Peter Karagiannis for reading the manuscript, and Hiromi Kishi, Minoru Okada, Akihiro Yamashita and Miho Morioka for assistance and helpful discussions. This study was supported in part by the Japan Science Technology Agency (JST), CREST (to N.T.), Scientific Research Grant No. 23792042 (to Y. M.) and No. 24390354 (to N.T.) from MEXT.

References

[1] H. Fujii, T. Sato, S. Kaneko, O. Gotoh, Y. Fujii-Kuriyama, K. Osawa, S. Kato, H. Hamada, Metabolic inactivation of retinoic acid by a novel P450 differentially expressed in developing mouse embryos, EMBO J. 16 (1997) 4163–4173.
[2] W.J. Ray, G. Bain, M. Yao, D.I. Gottlieb, CYP26, a novel mammalian cytochrome P450, is induced by retinoic acid and defines a new family, J. Biol. Chem. 272 (1997) 18702–18708.
[3] J.A. White, Y.D. Guo, K. Baetz, B. Beckett-Jones, J. Bonasoro, K.E. Hsu, F.J. Dilworth, G. Jones, M. Petkovich, Identification of the retinoic acid-inducible all-trans-retinoic acid 4-hydroxylase, J. Biol. Chem. 271 (1996) 29922–29927.
[4] S. Shimozono, T. Iimura, T. Kitaguchi, S. Higashijima, A. Miyawaki, Visualization of an endogenous retinoic acid gradient across embryonic development, Nature 496 (2013) 363–366.
[5] Y. Sakai, C. Meno, H. Fujii, J. Nishino, H. Shiratori, Y. Saijoh, J. Rossant, H. Hamada, The retinoic acid-inactivating enzyme CYP26 is essential for establishing an uneven distribution of retinoic acid along the anterio-posterior axis within the mouse embryo, Genes Dev. 15 (2001) 213–225.
[6] K. Yashiro, X. Zhao, M. Uehara, K. Yamashita, M. Nishijima, J. Nishino, Y. Saijoh, Y. Sakai, H. Hamada, Regulation of retinoic acid distribution is required for proximodistal patterning and outgrowth of the developing mouse limb, Dev. Cell 6 (2004) 411–422.
[7] F. Luthi, Y. Eggel, N. Theumann, Premature epiphyseal closure in an adolescent treated by retinoids for acne: an unusual cause of anterior knee pain, Joint Bone Spine 79 (2012) 314–316.
[8] L.M. Milstone, J. McGuire, R.C. Ablow, Premature epiphyseal closure in a child receiving oral 13-cis-retinoic acid, J. Am. Acad. Dermatol. 7 (1982) 663–666.
[9] J. Prendiville, E.A. Bingham, D. Burrows, Premature epiphyseal closure – a complication of etretinate therapy in children, J. Am. Acad. Dermatol. 15 (1986) 1259–1262.
[10] A.M. Standeven, P.J. Davies, R.A. Chandraratna, D.R. Mader, A.T. Johnson, V.A. Thomazy, Retinoid-induced epiphyseal plate closure in guinea pigs, Fundam. Appl. Toxicol. 34 (1996) 91–98.
[11] J.A. Williams, N. Kondo, T. Okabe, N. Takeshita, D.M. Pilchak, E. Koyama, T. Ochiai, D. Jensen, M.-L. Chu, M.A. Kane, J.L. Napoli, M. Enomoto-Iwamoto, N. Ghyselinck, P. Chambon, M. Pacifici, M. Iwamoto, Retinoic acid receptors are required for skeletal growth, matrix homeostasis and growth plate function in postnatal mouse, Dev. Biol. 328 (2009) 315–327.
[12] J.A. Williams, M. Kane, T. Okabe, M. Enomoto-Iwamoto, J.L. Napoli, M. Pacifici, M. Iwamoto, Endogenous retinoids in mammalian growth plate cartilage: analysis and roles in matrix homeostasis and turnover, J. Biol. Chem. 285 (2010) 36674–36681.
[13] J. Rossant, R. Zirngibl, D. Cado, M. Shago, V. Giguere, Expression of a retinoic acid response element-hsplacZ transgene defines specific domains of transcriptional activity during mouse embryogenesis, Genes Dev. 5 (1991) 1333–1344.
[14] T. Iwai, J. Murai, H. Yoshikawa, N. Tsumaki, Smad7 inhibits chondrocyte differentiation at multiple steps during endochondral bone formation and down-regulates p38 MAPK pathways, J. Biol. Chem. 283 (2008) 27154–27164.
[15] D. Ikegami, H. Akiyama, A. Suzuki, T. Nakamura, T. Nakano, H. Yoshikawa, N. Tsumaki, Sox9 sustains chondrocyte survival and hypertrophy in part through Pik3ca-Akt pathways, Development 138 (2011) 1507–1519.
[16] J. Okano, U. Lichti, S. Mamiya, M. Aronova, G. Zhang, S.H. Yuspa, H. Hamada, Y. Sakai, M.I. Morasso, Increased retinoic acid levels through ablation of Cyp26b1 determine the processes of embryonic skin barrier formation and peridermal development, J. Cell Sci. 125 (2012) 1827–1836.
[17] T. Kawamoto, Use of a new adhesive film for the preparation of multi-purpose fresh-frozen sections from hard tissues, whole-animals, insects and plants, Arch. Histol. Cytol. 66 (2003) 123–143.
[18] P.W.J. Peters, Double staining of fetal skeletons for cartilage and bone, in: H.J.M.D. Neuberg, T.E. Kwasigroch (Eds.), Methods in Prenatal Toxicology, Georg Thieme Verlag, Stuttgart, Germany, 1977, pp. 153–154.
[19] A.K. Verma, A. Shoemaker, R. Simsiman, M. Denning, R.D. Zachman, Expression of retinoic acid nuclear receptors and tissue transglutaminase is altered in various tissues of rats fed a vitamin A-deficient diet, J. Nutr. 122 (1992) 2144–2152.
[20] H.J. Dranse, A.V. Sampaio, M. Petkovich, T.M. Underhill, Genetic deletion of Cyp26b1 negatively impacts limb skeletogenesis by inhibiting chondrogenesis, J. Cell Sci. 124 (2011) 2723–2734.
[21] G. MacLean, H. Li, D. Metzger, P. Chambon, M. Petkovich, Apoptotic extinction of germ cells in testes of Cyp26b1 knockout mice, Endocrinology 148 (2007) 4560–4567.
[22] H.P. von Schroeder, J.N. Heersche, Retinoic acid responsiveness of cells and tissues in developing fetal limbs evaluated in a RAREhsplacZ transgenic mouse model, J. Orthop. Res. 16 (1998) 355–364.
[23] R.T. Ballock, X. Zhou, L.M. Mink, D.H. Chen, B.C. Mita, Both retinoic acid and 1,25(OH)2 vitamin D3 inhibit thyroid hormone-induced terminal differentiation of growth plate chondrocytes, J. Orthop. Res. 19 (2001) 43–49.
[24] M. Iwamoto, I.M. Shapiro, K. Yagami, A.L. Boskey, P.S. Leboy, S.L. Adams, M. Pacifici, Retinoic acid induces rapid mineralization and expression of mineralization-related genes in chondrocytes, Exp. Cell Res. 207 (1993) 413–420.
[25] M. Pacifici, E.B. Golden, M. Iwamoto, S.L. Adams, Retinoic acid treatment induces type X collagen gene expression in cultured chick chondrocytes, Exp. Cell Res. 195 (1991) 38–46.

ELSEVIER

CrossMark

The Spine Journal 15 (2015) 298–306

THE SPINE JOURNAL

Basic Science

Intermittent administration of teriparatide enhances graft bone healing and accelerates spinal fusion in rats with glucocorticoid-induced osteoporosis

Tsuyoshi Sugiura, MD, Masafumi Kashii, MD, PhD*, Yohei Matsuo, MD, Tokimitsu Morimoto, MD, Hirotsugu Honda, MD, PhD, Takashi Kaito, MD, PhD, Motoki Iwasaki, MD, PhD, Hideki Yoshikawa, MD, PhD

Department of Orthopedic Surgery, Faculty of Medicine, Graduate School of Medicine, Osaka University, 2-2 Yamadaoka, Suita, Osaka 565-0871, Japan

Received 7 March 2014; revised 7 July 2014; accepted 2 August 2014

Abstract

BACKGROUND CONTEXT: There has been no study regarding the effect of intermittent administration of teriparatide (TPTD [recombinant human parathyroid hormone (1-34)]) on spinal fusion in patients with glucocorticoid-induced osteoporosis (GIOP).

PURPOSE: To elucidate the effect of intermittent administration of TPTD on spinal fusion in rats with GIOP.

STUDY DESIGN: An experimental animal study of rats under continuous glucocorticoid (GC) exposure undergoing spinal fusion surgery and administration of TPTD or saline.

METHODS: Male 8-week-old rats (n=18) were administered 5 mg/kg methylprednisolone (MP) for 12 weeks. After 6 weeks of MP administration, the rats underwent posterolateral spinal fusion (L4–L5) with iliac crest autograft. Then, five times a week, they were given either saline or 40 μg/kg TPTD for 6 weeks. The following assessments were performed: time-course bone microstructural analysis of the fusion mass and adjacent vertebrae (L6), with in vivo microcomputed tomography (μCT); fusion assessment, with manual palpation testing and three-dimensional CT images; and bone histomorphometrical analysis of the fusion mass.

RESULTS: In the TPTD group, values for bone volume and other bone microstructural parameters at the fusion mass increased and peaked 4 weeks after surgery, and these values were significantly greater than those for the control (CNT) group at 4 and 6 weeks after surgery. Fusion assessment showed that fusion rate was higher in the TPTD group than in the CNT group (CNT group: 56%, TPTD group: 89%). Bone histomorphometry revealed that values for bone formation parameters were significantly higher in the TPTD group than in the CNT group.

CONCLUSIONS: Under continuous GC exposure in a rat model of spinal fusion, intermittent TPTD administration accelerated bone modeling and remodeling predominantly by stimulating bone formation at the fusion mass and increasing the fusion rate. Intermittent TPTD administration also improved bone microarchitecture of adjacent vertebrae.

Keywords: Teriparatide; Glucocorticoid-induced osteoporosis; Bone graft; Bone remodeling; Spinal fusion; Adjacent vertebrae

FDA device/drug status: Approved: Teriparatide, Methylprednisolone.

Author disclosures: ***TS:*** Nothing to disclose. ***MK:*** Nothing to disclose. ***YM:*** Nothing to disclose. ***TM:*** Nothing to disclose. ***HH:*** Nothing to disclose. ***TK:*** Nothing to disclose. ***MI:*** Nothing to disclose. ***HY:*** Nothing to disclose.

No funding sources supported this study. None of the authors has any financial interest in any of the commercial entities mentioned in this article.

* Corresponding author. Department of Orthopedic Surgery, Faculty of Medicine, Graduate School of Medicine, Osaka University, 2-2 Yamadaoka, Suita, Osaka 565-0871, Japan. Tel.: (81) 06-6879-3552; fax: (81) 06-6879-3559.

E-mail address: mkashii-osk@umin.ac.jp (M. Kashii)

http://dx.doi.org/10.1016/j.spinee.2014.08.001

Introduction

Glucocorticoids (GCs) are potent antiinflammatory and immunosuppressive agents widely used for the treatment of diseases such as asthma, chronic lung disease, rheumatoid arthritis and other connective tissue diseases, inflammatory bowel disease, and neuromuscular disease. However, clinical and experimental data have shown that prolonged GC exposure leads to trabecular bone loss and osteoporosis [1,2]. Prolonged exposure to GCs has the primary effect on decreasing bone formation because of the inhibition of the differentiation, activity, and life span of osteoblasts and osteocytes [3,4]. In one study, bone biopsies from those who received GCs showed a greater reduction in bone formation at the cellar and tissue levels compared with those with postmenopausal osteoporosis [5].

Spinal fusion surgery is one of the standard treatments for degenerative and traumatic spine diseases. In performing it, surgeons generally use bone grafting to restore mechanical stability to the affected spinal segment by bridging bone between the vertebrae, and successful bony union at unstable spine segments leads to pain relief and neurologic recovery [6–9]. Many authors have reported that spinal fusion in patients with osteoporosis carries a high incidence of surgical complications such as adjacent vertebral fractures of the surgical site or spinal instrumentation failure [10,11]. In particular, delayed union or pseudarthrosis of grafting bone, instrumentation failure, and adjacent vertebral fractures after surgery create more serious problems in performing spinal fusion surgery for patients with glucocorticoid-induced osteoporosis (GIOP) [12]. Depending on the pathophysiology of GIOP, pharmacological agents that stimulate bone formation and accelerate bone remodeling may hold the promise of resolving these problems.

Intermittent administration of parathyroid hormone (PTH) has a potent stimulatory effect on bone remodeling [13,14]. It has been reported that intermittent administration of teriparatide (TPTD or recombinant human PTH [1-34]) increases the cortical and cancellous bone mass, improves the microarchitecture of bone, and reduces the risk of osteoporotic vertebral fractures. Teriparatide has been widely used for the treatment of postmenopausal women and men with severe osteoporosis [15–17]. In addition, several randomized controlled clinical trials have shown the effectiveness of TPTD for treating GIOP, which was superior to that of antiresorptive bisphosphonates [18–20].

Teriparatide induces the maturation of circulating osteoblast precursors and differentiation of lining osteoblasts, stimulates the preexisting osteoblasts to form new bone, and reduces osteoblast and osteocyte apoptosis [21–23]. Teriparatide has potential as the ideal agent for resolving many problems regarding spinal fusion surgery in patients with GIOP, but there have been no studies on the effect of intermittent TPTD administration in spinal fusion in animals and patients with severe osteoporosis, such as GIOP. Thus, we conducted a study to elucidate whether intermittent TPTD administration stimulates graft bone healing in spinal fusion in GIOP in a rat model.

Methods

Animals

We purchased 8-week-old male Sprague-Dawley rats (n=21; mass, 260–285 g; purchased from SLC Japan, Hamamatsu, Japan). All rats were acclimated to an animal room at a controlled temperature (23°C±1°C) and humidity (45%–65%) and were housed in cages under specific pathogen-free conditions with a 12-hour light-dark cycle (light on, 0800–2000 hours). They were housed in cages under specific pathogen-free conditions with free access to water and standard laboratory feed (Oriental Yeast, Tokyo, Japan). Their housing and care and our experimental protocol were approved by the Animal Experimental Committee of Osaka University.

Chemicals and reagent

Methylprednisolone (MP) was purchased from Sigma-Aldrich (Tokyo, Japan) and dissolved in saline to 5 mg/kg. A powdered form of TPTD acetate (Asahi Kasei, Tokyo, Japan) was dissolved in saline to 40 μg/kg. For use in fluorescence labeling, calcein was purchased from Dojinwako (Tokyo, Japan).

Experiment design

Three rats were subcutaneously injected with saline per week for 6 weeks before surgery and were euthanized with an overdose of anesthetic agents as a baseline group. The other 18 rats were subcutaneously injected with MP five times per week at a dose of 5 mg/kg/d for 6 weeks before surgery. The dose of MP and dosing periods were determined on the basis of methods reported by Hulley et al. [24]. After 6 weeks of MP administration, rats were randomized into two groups before surgery; rats in the control group (CNT group; n=9) were given subcutaneous injections of 0.9% saline five times per week for 6 weeks and rats in the TPTD group (n=9) were given subcutaneous injections of 40 μg/kg/d of TPTD five times per week for 6 weeks. The dose of TPTD was determined according to the method used by Abe et al. [25]. After grouping, all rats were underwent posterolateral spinal fusion (L4–L5) with iliac crest autograft. Saline or TPTD injection started just after the surgery and continued for 6 weeks until the animals were euthanized, and MP administration also continued for 6 weeks until the animals were euthanized. All rats were weighed weekly, and the doses of MP and TPTD were adjusted accordingly. At 6 weeks after surgery, all rats were euthanized with an overdose of anesthetic agents.

Surgical procedures

Anesthesia was induced by subcutaneous injection of a cocktail of three drugs: 0.3 mg/kg of medetomidine (Nippon Zenyaku Kogyo Co., Ltd, Fukushima, Japan), 4 mg/kg of midazolam (Astellas Pharma, Inc., Tokyo, Japan), and 5 mg/kg of butorphanol tartrate (Meiji Seika Pharma Co., Ltd, Tokyo, Japan) [26]. After the surgical field was shaved and preprocessed, rats were placed in a prone position and then L4–L5 posterolateral fusion was performed as described elsewhere [25,27]. The spine was approached through a single midline skin incision and two paramedian fascial incisions. Spinal level was identified by referencing the iliac crests. After exposure, the transverse process and lateral gutters of the L4 and L5 vertebrae were decorticated with an electric bur until a blush of cancellous bone was observed. Approximately 0.2 g of corticocancellous bone was harvested from each iliac wing. The surgical sites were irrigated, and the harvested graft was placed into the fusion beds. The fascia and skin were closed with 3-0 nylon sutures. Postoperative antibiotics were given subcutaneously (penicillin G, 10,000 U/kg).

Time-course bone microstructural analysis

In all previous studies using an animal spinal fusion model, bone microstructural analysis of fusion mass was performed using image data from microcomputed tomography (μCT) after the animals were euthanized, which means that many animals had to be killed to perform time-course analysis. To reduce the number of rats required, we performed in vivo μCT (R_mCT; Rigaku, Tokyo, Japan) in our study. We analyzed the fusion mass between L4–L5 and the adjacent vertebra of the surgical site (L6) at 2, 4, and 6 weeks after surgery. Rats were anesthetized by subcutaneous injection of the anesthetic cocktail agents previously described. Scanning was initiated from the upper end plate of the L4 vertebrae to the lower end plate of the L6 vertebrae, with an isotropic voxel size of 59 μm. In vivo μCT was performed under consistent conditions (90 kV; 160 mA; irradiation time, 180 seconds). Cortical bone and trabecular bone were separated automatically, and bone microstructural parameters at the center of the fusion mass and the adjacent vertebra (L6) were assessed on three-dimensional images reconstructed using TRI/3D-BON (RATOC System Engineering, Tokyo, Japan). Bone volume (BV), BV/tissue volume (BV/TV), trabecular number (Tb.N), trabecular thickness (Tb.Th), and trabecular separation (Tb.Sp) were measured. In addition, bone mineral density (BMD) at the center of all L6 vertebrae was measured over time. We confirmed that the image quality of in vivo μCT was not inferior to that of in vitro μCT, by comparing the in vivo μCT images before euthanasia with in vitro μCT images just after euthanasia at 6 weeks postoperatively.

Fusion assessment

After the animals were euthanized, the lumbar spines were dissected and fixed with 70% ethanol, and nonligamentous soft tissues were cleaned. The harvested lumbar spines were gently palpated, and lateral side-bending motion at the L4–L5 level was compared with the motion at the adjacent levels above (L3–L4) and below (L5–L6). Manual palpation testing of the L4–L5 segments was performed by three independent observers who were unaware which segments were from the CNT group and which were from the TPTD group. This manual palpation method correlates well with more rigorous biomechanical testing in rabbit models and has been used to confirm spinal fusion in other studies [25,27,28]. We analyzed three-dimensional images reconstructed from μCT scans and determined whether the grafted bone had fused (Fig. 1). The specimen was graded as fused when formation of the bridging bone between the L4 and L5 transverse processes was clearly observed. Each specimen was given a grade of "union" when all observers graded it as fused in manual palpation testing or when all observers did not grade it as fused in manual palpation testing and as fused in our imaging study also.

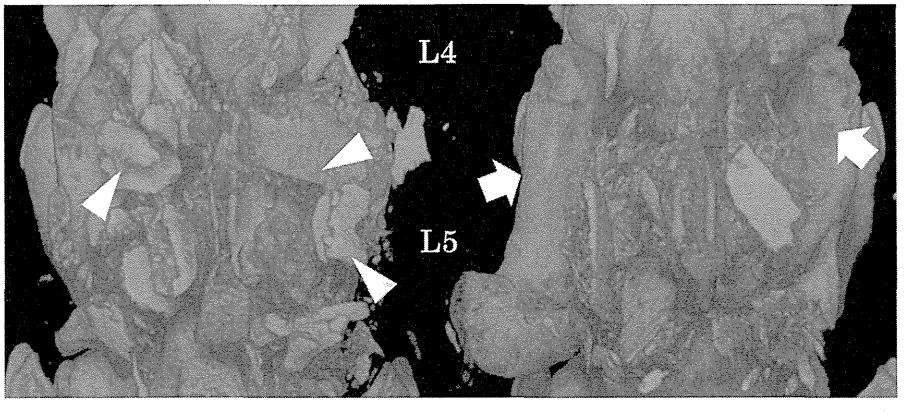

Fig. 1. Three-dimensional reconstruction images of the lumbar spine at L4–L5: (left) nonunion; (right) complete union. Formation of the bridging bone between L4 and L5 transverse processes was clearly observed in complete union specimens (white arrows). In contrast, fragments of grafted bone were more frequently observed in nonunion specimens (white triangles).

Bone histomorphometry

All rats were injected subcutaneously with 10 mg/kg calcein at 9 days and at 2 days before the animals were euthanized. Afterward, the dissected lumbar spines were fixed with 70% ethanol, stained with Villanueva bone stain, dehydrated through an ethanol series, and embedded in methyl methacrylate (Wako Chemicals, Kanagawa, Japan) without decalcification. After polymerization, the blocks were ground up to the transverse observation surface, perpendicular to the bone longitudinal direction at the fusion mass at the level of L4 inferior bony end plate of vertebra under CT image guidance (Fig. 2). Static and dynamic bone histomorphometrical measurements of the fusion mass were performed using a semiautomatic image-analyzing system (System Supply, Nagano, Japan) and a fluorescent microscope at magnifications of ×320.

We measured the following bone histomorphometrical parameters as described in the 2012 report of the American Society for Bone and Mineral Research Histomorphometry Nomenclature Committee [29]: osteoid and eroded surface per unit of bone surface (OS/BS and ES/BS), double-labeled and single-labeled surface per unit of bone surface (dLS/BS and sLS/BS), number of osteoblasts and osteoclasts per unit of bone surface (N.Ob/BS and N.Oc/BS), mineralizing surfaces (MS/BS), mineral apposition rate (MAR), and bone formation rate and resorption per unit of bone surface (BFR/BS and BFsR).

Serum bone metabolism markers

Blood samples were collected by cardiopuncture before the animals were euthanized; the samples were stored at −83°C for analyzing serum bone metabolism markers. Osteocalcin (OC), a bone formation marker, and tartrate-resistant acid phosphatase type 5b (TRACP-5b), a bone resorption marker, were analyzed using commercially available enzyme-linked immunosorbent assay kits (for the former, Rat Gla-Osteocalcin High Sensitive EIA Kit; Takara Bio, Shiga, Japan; for the latter, RatLaps EIA and RatTRAP Assay; Immunodiagnostic Systems Limited, Fountain Hills, AZ, USA) according to the manufacturers' protocols.

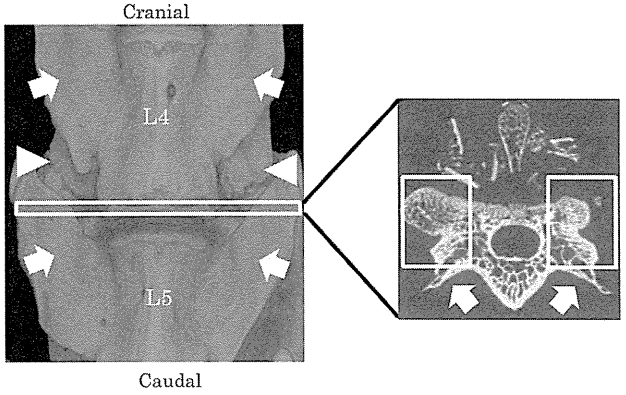

Fig. 2. Three-dimensional reconstruction image and cross-section of the region analyzed by bone histomorphometry (framed by white square). White arrows show transverse processes, and white triangles show grafted bone.

Statistical analysis

All data reported here are expressed as means and standard deviation. Comparison of values for microstructural parameters, histomorphometrical parameters, and serum bone metabolism marker levels between the TPTD and CNT groups were performed using the Student *t* test. Results of fusion assessment were compared using chi-square analysis. Probability values lower than .05 were considered to indicate statistical significance.

Results

Development of model rats with glucocorticoid-induced osteoporosis

This study was performed for the period of 3 months and no rats died in the study period.

After 5 mg/kg MP administration for 6 weeks, the rats' body weight increased 138.3±17.6 g from the first administration. Bone mineral density at vertebrae adjacent to the surgical site (L6) decreased approximately 20% compared with the baseline group that were not treated with MP (n=3). From these results, we confirmed that GIOP rats were successfully developed as described by Hulley et al. [24]. After surgery and administration of 5 mg/kg MP, there were no significant differences between the groups in body weight gain (CNT group, 46.7±18.4 g; TPTD group, 36.7±12.2 g; p=.19).

Bone microstructural parameters of fusion mass assessed by microcomputed tomography

Table 1 summarizes our findings for bone microstructural parameters of fusion mass. In the TPTD group, BV, BV/TV, and Tb.N at the fusion mass increased, reaching a peak at 4 weeks after surgery. Similarly, BV, BV/TV, and Tb.Th at the fusion mass gradually increased in the CNT group. BV/TV was significantly greater in the TPTD group than in the CNT group at 4 weeks, but the significant differences between the groups diminished by 6 weeks. BV and Tb.Th were significantly greater in the TPTD group than in the CNT group at 4 and 6 weeks after surgery. Tb.Sp tended to be lower in the TPTD group than in the CNT group at 2 and 4 weeks after surgery, but there were no significant differences between the two groups. Microcomputed tomography data of the fusion mass showed that the TPTD enhanced bone formation and accelerated bone absorption of graft bone secondary to bone formation.